



Article

Comparison of Seven Inversion Models for Estimating Plant and Woody Area Indices of Leaf-on and Leaf-off Forest Canopy Using Explicit 3D Forest Scenes

Jie Zou ^{1,2,3,*}, Yinguo Zhuang ¹, Francesco Chianucci ⁴ , Chunna Mai ¹, Weimu Lin ¹, Peng Leng ¹, Shezhou Luo ⁵ and Bojie Yan ⁶

¹ Spatial Information Research Center of Fujian Province, Fuzhou University, Fuzhou 350116, China; zhuang_yin_guo@163.com (Y.Z.); maichunna@163.com (C.M.); lin_weimu@163.com (W.L.); lengpeng_lp@163.com (P.L.)

² State Key Laboratory of Remote Sensing Science, Beijing Normal University, Beijing 100875, China

³ Key Laboratory of Data Mining and Information Sharing, Ministry of Education, Fuzhou 350116, China

⁴ CREA—Research Centre for Agriculture and Environment, via della Navicella 2-4, 00184 Rome, Italy; fchianucci@gmail.com

⁵ Key Laboratory of Digital Earth Science, Institute of Remote Sensing and Digital Earth, Chinese Academy of Sciences, Beijing 100094, China; luosz@radi.ac.cn

⁶ Department of Geography, Minjiang University, Fuzhou 350108, China; bnunercita@163.com

* Correspondence: zoujie@fzu.edu.cn; Tel.: +86-591-6317-9702

Received: 10 June 2018; Accepted: 9 August 2018; Published: 16 August 2018



Abstract: Optical methods require model inversion to infer plant area index (PAI) and woody area index (WAI) of leaf-on and leaf-off forest canopy from gap fraction or radiation attenuation measurements. Several inversion models have been developed previously, however, a thorough comparison of those inversion models in obtaining the PAI and WAI of leaf-on and leaf-off forest canopy has not been conducted so far. In the present study, an explicit 3D forest scene series with different PAI, WAI, phenological periods, stand density, tree species composition, plant functional types, canopy element clumping index, and woody component clumping index was generated using 50 detailed 3D tree models. The explicit 3D forest scene series was then used to assess the performance of seven commonly used inversion models to estimate the PAI and WAI of the leaf-on and leaf-off forest canopy. The PAI and WAI estimated from the seven inversion models and simulated digital hemispherical photography images were compared with the true PAI and WAI of leaf-on and leaf-off forest scenes. Factors that contributed to the differences between the estimates of the seven inversion models were analyzed. Results show that both the factors of inversion model, canopy element and woody component projection functions, canopy element and woody component estimation algorithms, and segment size are contributed to the differences between the PAI and WAI estimated from the seven inversion models. There is no universally valid combination of inversion model, needle-to-shoot area ratio, canopy element and woody component clumping index estimation algorithm, and segment size that can accurately measure the PAI and WAI of all leaf-on and leaf-off forest canopies. The performance of the combinations of inversion model, needle-to-shoot area ratio, canopy element and woody component clumping index estimation algorithm, and segment size to estimate the PAI and WAI of leaf-on and leaf-off forest canopies is the function of the inversion model as well as the canopy element and woody component clumping index estimation algorithm, segment size, PAI, WAI, tree species composition, and plant functional types. The impact of canopy element and woody component projection function measurements on the PAI and WAI estimation of the leaf-on and leaf-off forest canopy can be reduced to a low level (<4%) by adopting appropriate inversion models.

Keywords: plant area index (PAI); leaf area index (LAI); woody area index (WAI); clumping effect; inversion model; canopy element and woody component projection functions; digital hemispherical photography; forest canopy; forest scenes

1. Introduction

Understanding the energy and gas exchanges between forest ecosystems and the atmosphere is crucial in modeling terrestrial carbon cycle and global environmental change [1–4]. Leaf area index (LAI), which is defined as half of the total green leaf area per unit of flat ground area [5,6], is typically used to quantify the exchange between forest ecosystems and the atmosphere. LAI is a key parameter in biophysical and physiological processes, including photosynthesis, respiration, transpiration, carbon cycling, net primary productivity, and energy exchange. The LAI measurements of forest canopy are extensively used in many scientific areas, such as remote sensing, forestry, ecology, and global change [2,7,8].

Indirect methods are more frequently used than direct methods in estimating the LAI of leaf-on forest canopy because of their high efficiency, low cost, and nondestructive character [2,8,9]. Optical methods are amongst the most commonly used indirect methods, including LAI-2000/LAI-2200 (Li-Cor, Lincoln, NE, USA), digital hemispherical photography (DHP) [2,9], Tracing Radiation and Architecture of Canopies (TRAC) (3rd Wave Engineering, Winnipeg, Manitoba, Canada), DEMON (CSIRO, Canberra, Australia), and SunScan (Delta-T Devices, Cambridge, UK). Estimates obtained from optical methods rely upon the gap fraction measurements and inversion models. As most optical methods are unable to distinguish between leaves or shoots and woody components (e.g., stems, branches, flowers, and fruits), the estimates obtained from optical methods are often referred to as plant area index (PAI). PAI is the sum of LAI and woody area index (WAI).

Various inversion models have been proposed and applied to estimate the PAI and LAI of leaf-on forest canopy from optical methods, such as the Beer law or Poisson model [10–15], Miller theory [15–19], Look-Up Table (LUT) [15,20], and iterative optimization technique [21]. Amongst these inversion models, Miller theory and Beer law are the most widely used. Miller theory estimates the PAI and LAI of the leaf-on forest canopy by integrating the gap fraction measurements over the upper hemisphere or a specific zenith angle range. The iterative and optimization method estimates the PAI and LAI of the leaf-on forest canopy by searching the designed gap fraction values that closely match the measured gap fraction values, and the estimates calculated based on the target designed gap fraction are the PAI and LAI of the leaf-on forest canopy [21]. The LUT method estimates the PAI and LAI of the leaf-on forest canopy using the principle similar to the iterative and optimization method, but it simplifies the optimization process of the iterative and optimization method using a table with limited combinations of PAI, LAI, and gap fraction [15,20]. Different zenith angle ranges have been used by the aforementioned inversion models to estimate the LAI or PAI of leaf-on forest canopy from optical methods, such as 0–45° [22,23], 10–65° [18], 0–74° (five annulus, LAI-2000, or LAI-2200), 0~80° [16,17,22,24], 20–70° [25], 30–60° [22,26], and 57.3° [18,24,27,28]. For optical methods, such as LAI-2000 or LAI-2200 and DHP, various inversion models and zenith angle ranges were also employed to estimate the PAI or LAI of leaf-on forest canopy [10,17,18,22–26,29,30]. In addition to the PAI or LAI estimation, some studies attempted to obtain the effective woody area index (WAI_e) during leaf-off season to represent the WAI of the leaf-on forest canopy using optical methods, such as LAI-2000 [9,31,32] and DHP [22].

Previous studies showed that the PAI and LAI estimation of the leaf-on forest canopy from optical methods were largely affected by the applied inversion models and zenith angle ranges [15,16,18,22,23]. Significant differences were observed between the PAI and LAI which were estimated from different inversion models with the same zenith angle range [16,33], and from the same inversion model with different zenith angle ranges [18,22,24]. For example, Ryu et al. [33] pointed out large variations in the proportion between the effective plant area index (PAI_e) estimated from two inversion models

covered with the same zenith angle range at 41 forest sites with a range of 1–40%. Liu et al. [22] found that the variations in proportion between the PAI_e which were estimated from the four zenith angle ranges and Poisson model in a mixed broadleaved Korean pine forest canopy with a range of 0–37%. Therefore, the inversion model and zenith angle range play key roles in the PAI and LAI estimation of leaf-on forest canopy from optical methods. To date, no studies attempted to evaluate the impact of inversion models and zenith angle ranges on the estimation of WAI of the leaf-off forest canopy from optical methods. Considering the nonrandom distribution of the woody component of leaf-off forest canopy in space, which is similar to the spatial distribution of canopy element of leaf-on forest canopy, the inversion models and zenith angle ranges would be also the key factors that affect the WAI estimation of leaf-off forest canopy from optical methods.

Besides the inversion models and zenith angle ranges, the canopy element (G_e) and woody component (G_w) projection functions, needle-to-shoot area ratio (γ_e), and the canopy element (Ω_e) and woody component (Ω_w) clumping indices are also key issues in estimating the PAI and WAI of leaf-on and leaf-off forest canopy from the optical methods. The clumping effect of canopy element and woody component can be quantified by Ω_e and Ω_w , respectively. Moreover, they are often used to describe the degree of deviation from the random distribution of canopy element and woody component in space assumed by the inversion models [7,8,14]. If Ω_e and Ω_w are equal to unity this implies that the random distribution of the canopy element and woody component; if the distributions of the canopy element and woody component are clumped, then Ω_e and Ω_w are smaller than unity; and if the canopy element and woody component are regularly distributed, then Ω_e and Ω_w are larger than unity [7,8,14]. For coniferous forest canopy, the clumping effect of the canopy element is typically described in two scales: within and beyond-shoot clumping (Ω_e). The within-shoot clumping of coniferous forest canopy is quantified using the needle-to-shoot area ratio (γ_e), which is equal to unity for broadleaf forest canopy and larger than unity for coniferous forest canopy [34]. For coniferous forest canopy, γ_e can be estimated by taking the ratio of half the total needle area in a shoot to half the total shoot area [35]. The estimates obtained from optical methods are PAI_e and WAI_e , respectively, if the estimation does not consider γ_e , Ω_e and Ω_w . Previous studies reported that the PAI_e are usually 50–80% of PAI of leaf-on forest canopy [34]. Similarly, the spatial distribution of the woody component of stems and branches deviate from random distribution, therefore, Ω_w would be also the key factors affect the WAI estimation of leaf-off forest canopy from optical methods. Therefore, validating the aforementioned inversion models to estimate the PAI and WAI of leaf-on and leaf-off forest canopy should consider γ_e , Ω_e and Ω_w to achieve reliable and accurate conclusions. $G_e(\theta)$ and $G_w(\theta)$ are defined as the mean projection of unit surface area of the canopy element and woody component on the plane perpendicular to the view direction θ , and they can be estimated based on the canopy element and woody component angle distribution functions ($f(\theta_e)$ and $f(\theta_w)$, θ_e and θ_w are the canopy element and woody component inclination angles, respectively) [7,36,37]. The G_e and G_w of leaf-on and leaf-off forest canopy are site, species, and period specific [36,38,39]. The $G_e(\theta)$ and $G_w(\theta)$ usually vary with zenith angles ranging from 0° to 90° for real forest canopy, and approaching 0.5 at the zenith angle near 57.3° [7,36–38]. In previous studies, the $G_e(\theta)$ and $G_w(\theta)$ are often assumed to be 0.5 at all zenith angles ranging from 0° to 90° , even if the PAI and LAI estimation were not applied at this specific zenith angle of 57.3° due to difficulty in measuring the G_e and G_w of real forest canopy [22,24,25,35,40]. Woodgate et al. [37] reported that the LAI estimation errors introduced by ignoring G_w (based on the assumption that $G_w(0)$ equals 0.5) would be up to 25% at the leaf-on eucalypt canopy if the LAI was estimated at the zenith angle of 0° . Pisek et al. [36] reported that the assumption of spherical leaf angle distribution of the canopy element would result in LAI estimation errors of 28% to 47% at nadir for the leaf-on broad-leaved deciduous forest canopy. Therefore, G_e and G_w should not be ignored when evaluating the performance of inversion models to estimate the PAI and WAI of leaf-on and leaf-off forest canopy.

However, evaluating the impact of the factors of inversion model, zenith angle range, G_e , G_w , γ_e , Ω_e and Ω_w on the estimation of PAI and WAI of leaf-on and leaf-off forest canopy from optical methods

using direct methods is challenging and has rarely been conducted due to the disadvantages of the time-consuming, labor-intensive, and destructive character of direct methods. Recently, some studies attempted to assess the performance of optical methods to estimate the Ω_e , Ω_w , LAI and PAI of leaf-on and leaf-off forest canopy based on the 2D and 3D forest scenes and simulation method [18,20,26,41–45]. Compared with direct methods, the simulation method is affordable, nondestructive to forest canopy, and highly efficient. This method can generate forest scenes with contrasting canopy structure characteristics, which can extend beyond the limited sampling of field plots for direct methods. The measurements of optical methods can be generated within the forest scenes using the ray tracing algorithm [18,41]. The generated measurements would be beneficial to avoid major error sources in estimating the PAI_e and PAI of forest canopy from optical methods, such as classification of DHP images, determination of optimal exposure for imaging DHP images, lens distortion, and nonuniform sky conditions. Further, the true PAI and WAI, reference Ω_e and Ω_w , $G_e(\theta)$ and $G_w(\theta)$ can be accurately calculated based on the generated forest scenes. Therefore, it is an ideal tool for evaluating the reliability and performance of the inversion models, adopted by frequently used optical methods, to estimate the PAI and WAI of leaf-on and leaf-off forest canopy with consideration of G_e , G_w , γ_e , Ω_e and Ω_w . Several types of forest scenes, including the 2D (turbid media) [20,26,46] and quasi-3D forest scenes (geometric-optical models) [18], have been generated to validate the performance of inversion models in estimating the LAI and PAI of leaf-on and leaf-off forest canopy.

To date, few studies have attempted to assess the performance of inversion models for estimating the PAI of leaf-on forest canopy with consideration of G_e , G_w , γ_e , Ω_e and Ω_w based on the direct measurements of LAI from limited samples of field plots [16,22,24] and generated forest scenes [18,20,46]. The following three aspects have yet to be investigated or need further investigation:

- Two key components of leaf-on forest canopy, such as the needles of shoots and woody component, were not modeled by the forest scenes generated in previous studies [18,20,46]. However, these two components significantly affected the gap fraction measurements, thereby influencing the PAI and LAI estimation via optical methods [8,9,15,47]. Compared with the forest scenes in previous studies [20,26,46], the explicit 3D forest scenes in the present study provide a detailed description of all components of forest canopy, such as stems, branches, needles, shoots, leaves, flowers, and fruits, using a large number of small primitive shapes (e.g., triangles, cylinders, spheres, and ellipsoids) [48,49]. The explicit 3D tree models which were used to generate the explicit 3D forest scenes were constructed based on the field measurements of structural attributes (e.g., height, diameter at breast height [DBH], crown width, leaf length, leaf width, first branch height, and number of branch levels) of the tree canopy and available single-tree modeling methods (e.g., parametric and L-system-based modeling) [49,50]. Therefore, the explicit 3D forest scenes can provide leaf-on and leaf-off forest scenes with detailed description of canopy structure similar to the real leaf-on and leaf-off field plots as the optical methods undertaking [18]. The investigation and conclusions drawn based on the explicit 3D forest scene series would be more reliable and applicable.
- Although some studies attempted to assess the effect of inversion models on the PAI estimation of the leaf-on forest canopy, few commonly used inversion models were assessed by these studies, and the number of field plots covered were limited [16,18,22–24]. Moreover, the zenith angle dependent of Ω_e and G_e were not considered by some studies in evaluating the performance of inversion models to estimate the PAI of leaf-on forest canopy [20,22,24]. However, previous studies showed that the PAI and WAI estimation of the leaf-on and leaf-off forest canopy from optical methods was significantly affected by the Ω_e , Ω_w , G_e and G_w [15,18,34,36,45]; therefore, they should be considered in evaluating the performance of the inversion models to estimate the PAI and WAI estimation of the leaf-on and leaf-off forest canopy.
- The WAI estimation of the leaf-off forest canopy from optical methods is essential to derive the accurate LAI of the leaf-on forest canopy, as the latter is usually estimated by subtracting WAI

from PAI. So far, no study has attempted to evaluate the effect of inversion models on the WAI estimation of the leaf-off forest canopy through optical methods with consideration of Ω_w and G_w .

In this study, an explicit 3D forest scene series, which covered wide canopy structure characteristics with different PAI, WAI, Ω_e , Ω_w , phenological periods, stand density, tree species composition, and plant functional types, was generated to assess the performance of seven inversion models in estimating the PAI and WAI of leaf-on and leaf-off forest canopy, respectively. Considering the rare application of LUT and iterative optimization methods for estimating the PAI and WAI of leaf-on and leaf-off forest canopy in the field, we excluded these two methods from this study. Factors that contributed to the differences between the PAI or estimates of the seven inversion models were analyzed. The key factors that affect the performance of the seven inversion models in estimating the PAI and WAI of the leaf-on and leaf-off forest canopy were concluded. Finally, we attempted to identify the best combination of the inversion models, γ_e , Ω_e and Ω_w estimation algorithm, and segment size for estimating the PAI and WAI of leaf-on and leaf-off forest canopy.

2. Theory

The PAI of leaf-on forest canopy can be estimated based on the gap fraction and radiation attenuation measurements by inverting the Beer's law as described by Nilson [14] and Leblanc et al. [34]:

$$p_e(\theta) = \exp\left(\frac{-PAI\Omega_e(\theta)G_e(\theta)}{\cos(\theta)\gamma_e}\right) \quad (1)$$

where $p_e(\theta)$ is the measured canopy element gap fraction at θ , and $\Omega_e(\theta)$ is the canopy element clumping index at θ . The PAI cannot be inverted from Equation (1) if the $p_e(\theta)$ is equal to zero. In this study, the maximum value of PAI or PAI_e estimated at these zenith angles with gap fraction measurements equal to zero is assumed to be 10. $G_e(\theta)$ equals 0.5 at all zenith angles ranging from 0–90° if the canopy element angle distribution is assumed to be a spherical distribution. If $f(\theta_e)$ is known, then the $G_e(\theta)$ of the forest canopy can be calculated as follows:

$$G_e(\theta) = \int_0^{\frac{\pi}{2}} A(\theta, \theta_e) f(\theta_e) d\theta_e \quad (2a)$$

$$A(\theta, \theta_e) = \begin{cases} \cos \theta \cos \theta_e, & |\cot \theta \cot \theta_e| > 1 \\ \cos \theta \cos \theta_e [1 + (2/\pi)(\tan \psi - \psi)], & \text{otherwise} \end{cases} \quad (2b)$$

where $A(\theta, \theta_e)$ is the projection coefficient at the canopy element inclination angle of θ_e and the view zenith angle of θ and $\psi = \cos^{-1}(\cot \theta \cot \theta_e)$ [7].

To avoid the zenith angle dependence of PAI estimation on $G_e(\theta)$, Miller [19] proposed a theorem for the PAI estimation that does not require a prior knowledge of $G_e(\theta)$ (Miller_0-90) [18]:

$$PAI = -2 \int_0^{90} \frac{\ln[p_e(\theta)] \gamma_e}{\Omega_e(\theta)} \cos(\theta) \sin(\theta) d\theta \quad (3)$$

In addition to Miller_0-90, many studies suggested to estimate the PAI of the leaf-on forest canopy by inverting the Beer's law (Equation (1)) at a single zenith angle or narrow zenith angle range [16,18,24]:

$$PAI = -\frac{\ln(p_e(\theta')) \cos(\theta') \gamma_e}{G_e(\theta') \Omega_e(\theta')} \quad (4)$$

where θ' is the single zenith angle (or centered at an angle for a range of angles) for the PAI estimation. The $G_e(\theta)$ measurement of forest canopy using the direct methods, such as the manual clinometer and photography methods, is usually inapplicable in the field because of the limited qualified direct methods available for tall canopies and significant efforts required for the measurements [39]. However, previous studies reported that the $G_e(\theta)$ of the forest canopy is usually converged near the specific

zenith angle 57.3° and $G_e(57.3)$ equals ~ 0.5 [15,39,45]. If the θ' in Equation (4) is equal to or near 57.3° , then the PAI and WAI of forest canopy can be estimated by assuming the $G_e(57.3)$ in Equation (4) to be equal to 0.5 even if the $G_e(57.3)$ of the forest canopy is unknown (57.3) [15,39,45].

To avoid the sampling and optical errors at the zenith angles close to the zenith and horizon for the DHP method [17,26], many previous studies attempted to estimate the PAI_e and PAI of leaf-on forest canopy from the gap fraction measurements obtained at narrow zenith angle ranges by adopting the Miller theorem [17,18,22–26]. The sampling areas covered by the annulus of DHP images with center zenith angles near 0° are much smaller than those with center zenith angles near 90° . Therefore, the incomplete sampling of forest canopy for the annulus with center zenith angles near 0° would further result in estimation uncertainties in the PAI_e , PAI, and Ω_e estimation [40]. In addition, the image pixels of annuli with center zenith angles near 0° are prone to overexposure compared with those close to 90° . More light can penetrate through the canopy from above to the sensor for the annuli with center zenith angles near 0° compared with 90° due to the larger gaps viewed by and the shorter extinct path length for those annuli. The zenith angles close to 90° were also usually discarded for the PAI_e and PAI estimation of the leaf-on forest canopy due to the presence of mixed pixels, absence of gaps, significant contribution of woody components, and interference of ground. The annulus with center zenith angles close to 90° tended to have a high proportion of mixed pixels due to the coarse image resolution and light scattering [41]. The high proportion of mixed pixels would reduce the classification accuracy of DHP images and further make the PAI_e and PAI estimates unreliable. Moreover, the DHP method tended to produce null gap fraction measurements at the annuli with center zenith angles close to 90° in dense forest canopy [25]. This situation would produce estimation errors in the PAI estimation because it requires a definition of the logarithm of zero, $p_e(\theta)$, which is not defined [51]. The ground would be visible in the annuli with center zenith angles close to 90° if the ground slope of the plot is larger than zero [52]. The annuli with visible ground are usually discarded to remove the interference of ground to the PAI_e and PAI estimation [52]. For the aforementioned reasons, Leblanc and Fournier [18] attempted to estimate the PAI of the leaf-on forest canopy based on the Miller theorem and the gap fraction measurements obtained at the zenith angle range of $10\text{--}65^\circ$ (Miller_10-65):

$$PAI = -2 \int_{10}^{65} \frac{\ln[p_e(\theta)]\gamma_e}{G_e(\theta)\Omega_e(\theta)} \cos(\theta) \sin(\theta) d\theta \quad (5)$$

Similarly, the PAI of the leaf-on forest canopy can be estimated based on the Miller theorem and the gap fraction measurements obtained at another zenith angle range which enlarges the zenith angle range of $10\text{--}65^\circ$ to $0\text{--}80^\circ$, and the zenith angles close to horizon are discarded for the abovementioned reasons (Miller_0-80) [24]:

$$PAI = -2 \int_0^{80} \frac{\ln[p_e(\theta)]\gamma_e}{G_e(\theta)\Omega_e(\theta)} \cos(\theta) \sin(\theta) d\theta \quad (6)$$

The LAI-2000 or LAI-2200 instrument estimates the PAI of the leaf-on forest canopy based on the Miller theorem and the gap fraction measurements obtained from five annuli, and the gap fraction measurements of the fifth annulus is used to complete the zenith angle up to 90° (LAI-2200) [29,30]:

$$PAI = -\sum_{i=1}^5 \frac{\ln[p_{e_i}(\theta_i)] \cos(\theta_i) \gamma_e W_i}{G_{e_i} \Omega_{e_i}} \quad (7)$$

where θ_i is the center zenith angle of the i th annulus, $p_{e_i}(\theta_i)$ is the canopy element gap fraction of the i th annulus, Ω_{e_i} and G_{e_i} are the Ω_e and G_e estimates of the i th annulus and W_i is the weight factor of the i th annulus. The five zenith angle ranges used in Equation (7) are the same as the zenith angle

ranges covered by the five concentric annuli of the LAI-2000 or LAI-2200 instrument; these zenith angle ranges are 0–13°, 16–28°, 32–43°, 47–58°, and 61–74°. The equation for W_i is as follows:

$$W_i = \sin(\theta_i)d\theta_i \quad (8)$$

when normalized to 1.0, the values of W_i in Equation (7) are 0.041, 0.131, 0.201, 0.29, and 0.337, which correspond to the five annuli with the center zenith angles of 7°, 23°, 38°, 53° and 68°, respectively [29,30].

Moreover, the PAI of the leaf-on forest canopy can be estimated based on DHP images using the calculation method similar to the LAI-2200 instrument by evenly dividing the zenith angle ranges from 0° to 81° and from 0° to 90° into 9 and 10 annuli (DHP_0-81 and DHP_0-90) [8]:

$$PAI = - \sum_{i=1}^9 \frac{\ln[p_{e-i}(\theta_i)] \cos(\theta_i) \gamma_e W_i}{G_{e-i} \Omega_{e-i}} \quad (9)$$

$$PAI = - \sum_{i=1}^{10} \frac{\ln[p_{e-i}(\theta_i)] \cos(\theta_i) \gamma_e W_i}{G_{e-i} \Omega_{e-i}} \quad (10)$$

The calculation method of W_i used in Equations (9)–(10) is the same as the method of LAI-2200 (Equation (8)). The normalized W_i values of the nine zenith angle ranges in Equation (9) are 0.0124, 0.0367, 0.0602, 0.0823, 0.1023, 0.1198, 0.1343, 0.1455, and 0.3064, respectively. The normalized W_i values of the 10 zenith angle ranges in Equation (10) are 0.0123, 0.0366, 0.0601, 0.0820, 0.1019, 0.1193, 0.1338, 0.1450, 0.1526, and 0.1564, respectively.

If the PAI of the leaf-on forest canopy is known, then the reference Ω_e of the leaf-on forest canopy can be estimated as follows:

$$\Omega_e = \frac{PAI_e}{PAI} \quad (11)$$

In this study, the estimates derived from the seven inversion models of Miller_0-90, 57.3, Miller_10-65, Miller_0-80, LAI-2200, DHP_0-81, and DHP_0-90 (Equations (3)–(7) and (9)–(10)) are PAI_e , namely, $PAI_{e_Miller_0-90}$, $PAI_{e_57.3}$, $PAI_{e_Miller_10-65}$, $PAI_{e_Miller_0-80}$, $PAI_{e_LAI-2200}$, $PAI_{e_DHP_0-81}$, and $PAI_{e_DHP_0-90}$, respectively, if γ_e or $\Omega_e(\theta)$ is assumed to be equal to 1 in the PAI estimation of leaf-on forest canopy. Similarly, the estimates derived from the seven inversion models of Miller_0-90, 57.3, Miller_10-65, Miller_0-80, LAI-2200, DHP_0-81, and DHP_0-90 (Equations (3)–(7) and (9)–(10)) are WAI_e , namely, $WAI_{e_Miller_0-90}$, $WAI_{e_57.3}$, $WAI_{e_Miller_10-65}$, $WAI_{e_Miller_0-80}$, $WAI_{e_LAI-2200}$, $WAI_{e_DHP_0-81}$, and $WAI_{e_DHP_0-90}$, respectively, if $\Omega_w(\theta)$ is assumed to be equal to 1 in the WAI estimation of leaf-off forest canopy. The equations used for estimating the WAI and reference Ω_w of the leaf-off forest canopy are the same as those for PAI and reference Ω_e (Equations (3)–(7) and (9)–(11)), respectively.

3. Materials and Methods

3.1. Generation of Explicit 3D Forest Scenes and DHP Images

In this study, the explicit 3D forest scenes were generated based on a series of 50 detailed 3D tree models selected from all the 46 detailed 3D tree models in the four forest scenes, namely, Järvelja pine stand (summer) (JPSS), Ofenpass pine stand (winter) (OPSW), Järvelja birch stand (summer) (JBSS), and Järvelja birch stand (winter) (JBSW), in the fourth radiation transfer model intercomparison (RAMI) project (<http://rami-benchmark.jrc.ec.europa.eu/HTML/RAMI-IV/RAMI-IV.php>) except the Norway spruce (*Picea abies*) tree model in JBSS and the birch (*Betula pendula*) tree model in JPSS. Another six Scots pine (*Pinus sylvestris*) models, which were used by Disney et al. [53], were also used in generating the forest scenes in the present study. These detailed 3D tree models provide a detailed description of the canopy elements of tree canopy, including leaves or shoots, branches, and stems.

An in-house software product called In situ LAI Measurements Simulation and Validation Platform (ILMSVP, version 2016) (Appendix B) was developed using the C++ programming language. This software was used to generate the explicit 3D forest scene series and simulated DHP images. The generated leaf-on forest scenes comprise the leaf-on broadleaved deciduous and evergreen coniferous forest scenes, and the leaf-off forest scenes are the leaf-off broadleaved deciduous forest scenes. The leaf-on deciduous forest scenes were generated using ILMSVP based on all the broadleaf 3D tree models from JBSS. To avoid the true LAI values of the generated leaf-on deciduous forest scenes are far larger than the maximum LAI of 4.76 for the birch plot, as reported by Sumida et al. [54], those scenes with LAI > 5.0 were discarded and excluded from this study. In addition, all the leaves were removed from the tree models in the sub-series deciduous scenes of JBSS to represent the leaf-off period of the sub-series deciduous scenes of JBSS (JBSW). Amongst the six broadleaf tree species of maple (*Acer Platanoides*), birch (*Betula Pendula*), alder (*Alnus Glutinosa*), linden (*Tilio Cordata*), poplar (*Populus Tremuloides*), and ash (*Fraxinus Exelsior*) in JBSS, the birch tree species is the dominant species. Therefore, the leaf-on and leaf-off broadleaved deciduous forest scenes can be treated as the birch forest scenes. The leaf-on coniferous forest scenes were generated using ILMSVP based on all needleleaf 3D tree models from JPSS, OPSW, and six Scots pine models, respectively. Therefore, three sub-series of leaf-on coniferous scenes were generated, namely JPSS, OPSW, and Scots pine scenes (SPS). Similar to the leaf-on deciduous scenes, all the PAI of the generated two sub-series coniferous scenes of SPS and OPSW were below the maximum PAI of 7.8 and 1.9 of the Scots pine and Mountain pine forest sites, respectively, as reported by Walter [55] and Thimonier et al. [23], respectively. The two 3D tree models of the Norway spruce and birch were not used in generating the two sub-series coniferous scenes of JBSS and JPSS, respectively, for the purpose of generating pure deciduous and coniferous forest scenes. Because the proportions of the number of Norway spruce and birch trees to the total number of trees in JBSS and JPSS are as small as 3% and 0.5%, respectively. Therefore, the removal of the two 3D tree models of Norway spruce and birch in the generation of the two sub-series coniferous scenes of JBSS and JPSS would not make the main canopy structural characteristics of the two sub-series coniferous scenes of JBSS and JPSS deviate obviously from those of the two scenes of JBSS and JPSS in RAMI project, respectively. In this study, a total of 156 forest scenes were constructed based on the 50 detailed 3D tree models described. The four scenes of JPSS, OPSW, JBSS, and JBSW in the RAMI project were also used in this study. These forest scenes are reclassified into two types: leaf-on and leaf-off. The number of leaf-on and leaf-off forest scenes were 106 and 54, respectively. Table 1 provides the main characteristics of the simulated 3D forest scene series. The frequency distributions of the true PAI and WAI (a), and the reference Ω_e and Ω_w (b) of the simulated leaf-on and leaf-off forest scenes are shown in Figure 1. Figure 2 shows two simulated binary DHP images generated at the same sampling point at leaf-on and leaf-off periods of a deciduous forest scene.

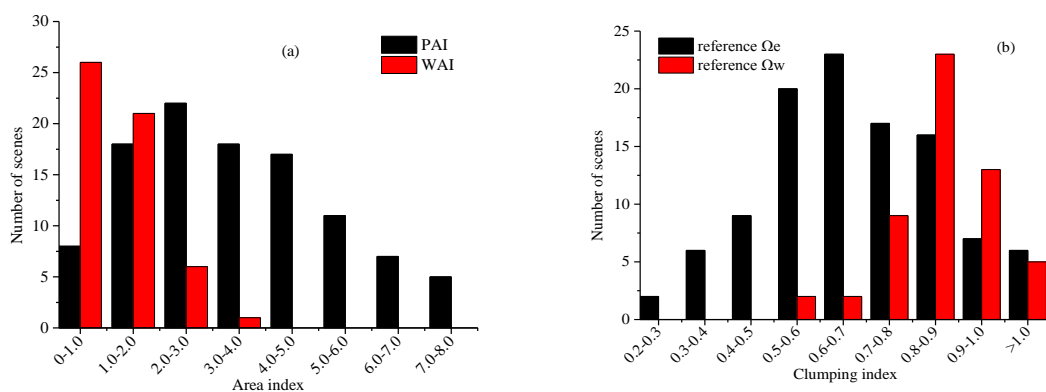


Figure 1. Frequency distributions of true PAI and WAI (a), and reference Ω_e and Ω_w (b) of leaf-on and leaf-off forest scenes, respectively.

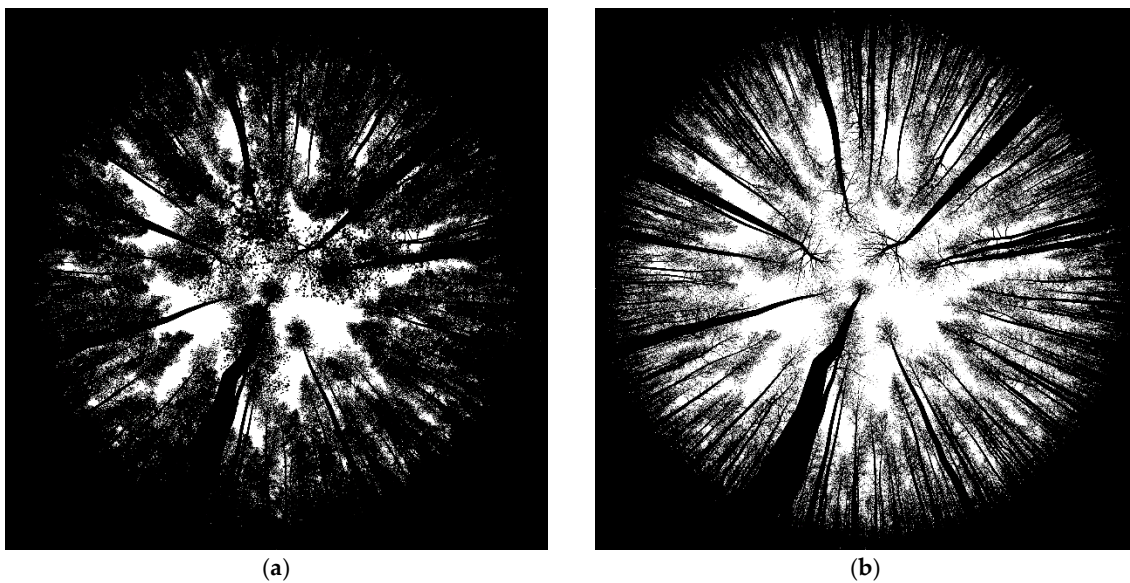


Figure 2. Two simulated binary DHP images generated at the same sampling point at leaf-on (a) and leaf-off (b) periods of a deciduous forest scene.

Table 1. Main characteristics of simulated explicit 3D forest scene series (JBSS: Järvelja birch stand [summer], JBSW: Järvelja birch stand [winter], JPSS: Järvelja pine stand [summer], OPSW: Ofenpass pine stand [winter], SPS: Scots pine scenes, WAI: woody area index, LAI: leaf area index, Ω_e : canopy element clumping index, and γ_e : needle-to-shoot area ratio).

Plant Function Types	Broadleaved Deciduous Scenes		Evergreen Coniferous Scenes		
Sub-series scenes	JBSS	JBSW	JPSS	OPSW	SPS
Phenological period	Leaf-on	Leaf-off		Leaf-on	
Dominant species	<i>Betula pendula</i>		<i>Pinus sylvestris</i>	<i>Pinus montana</i>	<i>Pinus sylvestris</i>
WAI	0.10–3.53		0.46–1.63	0.06–0.76	0.31–3.16
PAI	0.51–8.0	0.10–3.53 *	1.52–5.86	0.59–2.64	2.06–7.26
Reference Ω_e	0.39–0.92	0.55–1.30 **	0.55–0.96	0.20–1.03	0.48–1.35
γ_e	1		1.32	1.48	2.12
Mean tree height (m)	8.91–23.0		12.32–15.55	3.53–9.92	4.78–10.26
Tree species composition	6		1	1	1
Number of scenes	54	54	21	19	12
Stand density (stems ha ⁻¹)	250–3000	250–3000	550–2800	500–2150	550–4000
Stem distribution mode	Random, Regular, Clumped, Natural				

* For leaf-off JBSW scenes, the PAI equals WAI. ** For leaf-off JBSW scenes, the reference Ω_e equals reference Ω_w .

3.2. Data Processing

The true LAI or WAI of each generated leaf-on and leaf-off forest scene were calculated by taking the ratio between half of the total surface areas of triangles, cylinders, and ellipsoids of the leaves and needles or the stems and branches in the scenes and the flat ground area of the forest scene. The true PAI of the scenes is the sum of the LAI and WAI values. For leaf-off forest scenes, the PAI is equal to the WAI. The $f(\theta_e)$ of each leaf-on forest scene was calculated by dividing the total surface area of leaves or shoots, stems, and branches in the scene by the sum of the surface area of leaves or shoots, stems, and branches with inclination angles ranging from $\theta_e - 0.5^\circ$ to $\theta_e + 0.5^\circ$, except at the two zenith angles of 0° and 90° . The two zenith angle ranges of 0° to 0.5° and 89.5° to 90° were used to estimate the $f(0)$ and $f(90)$ of leaf-on forest scenes, respectively. Thereafter, the $G_e(\theta)$ of each leaf-on forest scene was calculated at the zenith angle range of 0 – 90° with an interval of 1° by substituting the $f(\theta_e)$ into Equation (2). The calculation method of the $f(\theta_w)$ and $G_w(\theta)$ of each leaf-off forest scene is the same to the $f(\theta_e)$ and $G_e(\theta)$ of each leaf-on forest scene. For the three inversion models of LAI-2200, DHP_0-81 and DHP_0-90, the G_{e_i} and G_{w_i} were calculated by averaging the $G_e(\theta)$ and $G_w(\theta)$ at the

zenith angle ranges covered by the i th annulus. The γ_e of each leaf-on coniferous forest scene was calculated by taking the ratio between half of the total needle area in a shoot to half of the shoot surface area. The shoot surface area was estimated using the projection method described by Chen [35].

For each scene, the $p_e(\theta)$ was calculated by dividing the total number of black and white pixels by the total number of white pixels with zenith angles ranging from $\theta - 0.5^\circ$ to $\theta + 0.5^\circ$, except at the two zenith angles of 0° and 90° . The zenith angle ranges, which were used to calculate the $p_e(0)$ and $p_e(90)$, are the same as the two zenith angle ranges used to estimate the $f(\theta_e)$ and $f(\theta_w)$ of the leaf-on and leaf-off forest scenes, respectively. For the three inversion models of LAI-2200, DHP_0-81, and DHP_0-90, the calculation procedures of $p_{e_i}(\theta_i)$ in each scene are similar to those of $p_e(\theta)$. The only difference is that $p_{e_i}(\theta_i)$ was calculated based on the total number of black and white pixels with zenith angles covered by the i th annulus. In this study, the $p_e(\theta')$ of the 57.3° inversion model was calculated based on the total number of black and white pixels with zenith angles ranging from 52 – 62° . The calculation procedures of $p_w(\theta)$, $p_{w_i}(\theta_i)$, and $p_w(\theta')$ are the same as the $p_e(\theta)$, $p_{e_i}(\theta_i)$, and $p_e(\theta')$ estimation. The only difference is that the $p_w(\theta)$, $p_{w_i}(\theta_i)$, and $p_w(\theta')$ were estimated using the simulated binary DHP images of leaf-off deciduous forest scenes.

All the simulated binary DHP images were processed using the Measurement Tools of Vegetation Structural Parameters software (MTVSP, version 2015) [56] to calculate the Ω_e and Ω_w of the leaf-on and leaf-off forest scenes, respectively. Several previous studies attempted to evaluate the performance of various algorithms to estimate the Ω_e and Ω_w of leaf-on and leaf-off forest canopy based on DHP images, respectively. However, these studies only focused on estimating the $\Omega_e(\theta)$ and $\Omega_w(\theta)$ at the single zenith angle near 57.3° [18] or narrow zenith angle range of 30 – 60° [41] and the impact of different Ω_e estimation algorithms on the estimation of PAI was not analyzed [45]. As the performance of inversion models to estimate the PAI and WAI of leaf-on and leaf-off forest canopy is inexorably linked to the performance of the Ω_e and Ω_w estimation algorithm used and the zenith angle dependence of $\Omega_e(\theta)$ and $\Omega_w(\theta)$. Therefore, the Ω_e and Ω_w estimation algorithms and parameters suggested by these studies were not used directly in the present study. In this study, four commonly used Ω_e and Ω_w estimation algorithms, including gap fraction and gap-size based algorithms (logarithmic averaging (LX) [57], gap size distribution (CC) [58,59], combination of gap size and logarithmic averaging (CLX) [17]), and Pielou's coefficient of spatial segregation (PCS) [43] were used to estimate the Ω_e and Ω_w of the leaf-on and leaf-off forest scenes, respectively. For simplicity, the modified gap size distribution (CMN) [60] and modified logarithmic averaging (LXW) [41] algorithms were not assessed in this study due to the high similarity between CC and CMN, and between LX and LXW. For CLX, three segment sizes of 15° , 30° , and 45° were used in this study. These three segment sizes covered the two segment sizes of 15° and 45° , as suggested by Woodgate [45] and Leblanc et al. [18], respectively. No segment sizes larger than 45° were used in this study as CLX tended to produce worse Ω_e and Ω_w estimates with large segment sizes [45]. For LX, three segment sizes of 5° , 15° , and 30° were used in this study. The three segment sizes covered the segment size of 5° suggested by Gonsamo et al. [26] to estimate Ω_e from DHP images using LX. We did not use segment sizes larger than 30° for LX to estimate the Ω_e and Ω_w of the leaf-on and leaf-off scenes as canopy element and woody component usually tended to be nonrandomly distributed at the scale of segment with large segment sizes.

Eight $\Omega_e(\theta)$ and $\Omega_w(\theta)$ estimates were calculated based on the four algorithms (one estimate each for the CC and PCS algorithms, and three estimates each for the LX and CLX algorithms) at each zenith angle with zenith angles ranging from 10 – 90° with interval of 1° . The $\Omega_e(\theta)$ and $\Omega_w(\theta)$ with zenith angles ranging from 0 – 9° were not calculated based on the DHP images directly due to reasons mentioned above and the limited and insufficient gap size measurements collected at these small zenith angles. Woodgate [45] reported that the reference $\Omega_e(\theta)$ of the leaf-on eucalypt forest scenes at zenith angles ranging from 7 – 75° were almost constant, and the $\Omega_e(\theta)$ estimated using CLX (segment sizes of 15° , 45° , and 90°) at zenith angles near 10° are very close to the reference Ω_e of the scenes. In this study, to obtain the 91 $\Omega_e(\theta)$ and $\Omega_w(\theta)$ estimates that match the $p_e(\theta)$ and $p_w(\theta)$ measurements at the same zenith angle range of 0 – 90° with an interval of 1° , we treated the $\Omega_e(\theta)$ and

$\Omega_w(\theta)$ at the 10 zenith angles in the range of 0–9° with the interval of 1° as equal to the $\Omega_e(\theta)$ and $\Omega_w(\theta)$ at the 10° zenith angle, respectively. For the three inversion models of LAI-2200, DHP_0-81, and DHP_0-90, the Ω_{e_i} and Ω_{w_i} were calculated by averaging the $\Omega_e(\theta)$ and $\Omega_w(\theta)$ estimates with the zenith angles covered by the i th annulus with an interval of 1°, respectively. Similarly, the $\Omega_e(\theta')$ and $\Omega_w(\theta')$ of the 57.3 inversion model were calculated by averaging the $\Omega_e(\theta)$ and $\Omega_w(\theta)$ with zenith angles ranging from 52–62° with an interval of 1°.

After the calculation of $p_e(\theta)$, $p_w(\theta)$, $p_{e_i}(\theta_i)$, $p_{w_i}(\theta_i)$, $p_e(\theta')$, $p_w(\theta')$, γ_e , $G_e(\theta)$, $G_w(\theta)$, G_{e_i} , G_{w_i} , $\Omega_e(\theta)$, $\Omega_w(\theta)$, Ω_{e_i} , and Ω_{w_i} for each scene, the PAI_e , PAI , WAI_e , and WAI estimates of each leaf-on and leaf-off scene were calculated from the seven inversion models using Equations (3)–(7), (9) and (10), respectively. The reference Ω_e and Ω_w of leaf-on and leaf-off scenes were calculated using Equation (11) based on the true PAI and WAI of leaf-on and leaf-off scenes, and the $PAI_{e_{57.3}}$ and $WAI_{e_{57.3}}$ which were derived using the 57.3 inversion model without consideration of G_e , G_w , γ_e , Ω_e , and Ω_w , respectively. Hereinafter, if the G_e and G_w , γ_e , and Ω_e and Ω_w were stated not considered in the PAI_e , PAI , WAI_e , and WAI estimation, then the statement means that the assumption of spherical projection function was made for G_e and G_w , and the γ_e , $\Omega_e(\theta)$, and $\Omega_w(\theta)$ are assumed to be equal to 1.

In this study, for convenience, we classified the factors that contributed to the differences between the PAI_e , PAI , WAI_e , and WAI estimates of the seven inversion models as the inversion model, G_e and G_w , γ_e , Ω_e and Ω_w estimation algorithm, and segment size. Hereinafter, the Equations of (3)–(7), (9) and (10) were treated as the factor of the inversion model that contributed to the differences between the estimates derived from the seven inversion models, excluding the part of $G_e(\theta)$, $G_e(\theta')$, G_{e_i} , γ_e , $\Omega_e(\theta)$, $\Omega_e(\theta')$, and Ω_{e_i} .

4. Results

4.1. Factors Contributing to Differences between PAI_e or WAI_e , Which Were Derived from Seven Inversion Models

4.1.1. Inversion Model

Figure 3 shows that the mean $p_e(\theta)$ of the leaf-on scenes and the mean $p_w(\theta)$ of the leaf-off scenes tended to decrease obviously with the increase of zenith angles at the zenith angle range of 0–90° and they approach zero at zenith angles larger than 85°. Table 2 shows the mean PAI_e of all the leaf-on coniferous and deciduous scenes, and the mean WAI_e of all the leaf-off deciduous scenes, which were derived from the seven inversion models with the assumption of the spherical projection function of G_e and G_w . The mean $PAI_{e_{Miller_10-65}}$ and $WAI_{e_{Miller_10-65}}$ were smaller than those mean PAI_e and WAI_e estimates calculated from other six inversion models, respectively (Table 2). By contrast, the mean $PAI_{e_{Miller_0-90}}$ and $WAI_{e_{Miller_0-90}}$ were larger than those mean PAI_e and WAI_e estimates calculated from the other six inversion models except 57.3, respectively (Table 2). The mean $PAI_{e_{Miller_0-90}}$ and $WAI_{e_{Miller_0-90}}$ were approximately two times $PAI_{e_{Miller_10-65}}$ and $WAI_{e_{Miller_10-65}}$, respectively (Table 2). Large differences were also observed between the mean $PAI_{e_{Miller_0-80}}$ and $PAI_{e_{Miller_0-90}}$ or $WAI_{e_{Miller_0-80}}$ and $WAI_{e_{Miller_0-90}}$. For example, the mean $PAI_{e_{Miller_0-90}}$ were 42% and 33% larger than $PAI_{e_{Miller_0-80}}$ in the leaf-on coniferous and deciduous scenes, respectively (Table 2). Similarly, the mean $WAI_{e_{Miller_0-90}}$ were 24% larger than $WAI_{e_{Miller_0-80}}$ in the leaf-off deciduous scenes (Table 2). Compared with Miller_0-80 and Miller_0-90, no large differences were observed between the mean PAI_e or WAI_e estimates of DHP_0-81 and DHP_0-90 at the leaf-on and leaf-off forest scenes, even when the same zenith angle ranges were covered by the two groups of inversion models (Table 2). The variations in proportion between the mean $PAI_{e_{DHP_0-81}}$ and $PAI_{e_{DHP_0-90}}$ or $WAI_{e_{DHP_0-81}}$ and $WAI_{e_{DHP_0-90}}$ estimates are below 6%. The variations in proportion between the mean $PAI_{e_{Miller_0-90}}$ and $PAI_{e_{DHP_0-90}}$ or $WAI_{e_{Miller_0-90}}$ and $WAI_{e_{DHP_0-90}}$ estimates are 22%, 18%, and 9% in the leaf-on coniferous, leaf-on deciduous, and leaf-off deciduous scenes, respectively (Table 2).

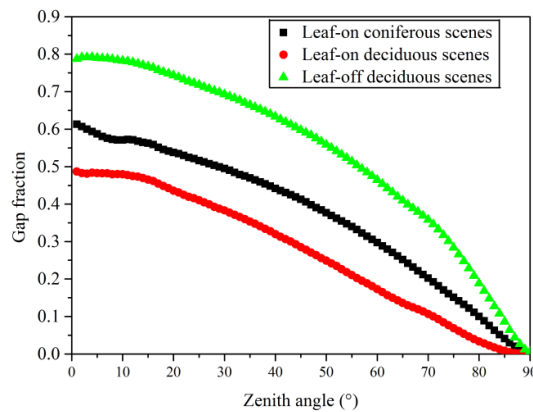


Figure 3. The mean $p_e(\theta)$ and $p_w(\theta)$ of leaf-on and leaf-off forest scenes, which were derived by averaging the $p_e(\theta)$ and $p_w(\theta)$ of all scenes at zenith angles in the 0–90° range with interval of 1°.

Table 2. Mean PAI_e of leaf-on coniferous and deciduous scenes and mean WAI_e of leaf-off deciduous scenes derived from seven inversion models using Equations (3)–(7), (9) and (10) by assuming $G_e(\theta)$ and $G_w(\theta)$ to be equal to 0.5 ($\gamma_e, \Omega_e(\theta), \Omega_w(\theta), \Omega_e(\theta'), \Omega_w(\theta'), \Omega_{e_i}$, and Ω_{w_i} are assumed to be equal to 1).

Inversion Model	Miller_10-65	Miller_0-80	Miller_0-90	LAI_2200	DHP_0-81	DHP_0-90	57.3
	$PAI_{e_Miller_10-65}$	$PAI_{e_Miller_0-80}$	$PAI_{e_Miller_0-90}$	$PAI_{e_LAI-2200}$	$PAI_{e_DHP_0-81}$	$PAI_{e_DHP_0-90}$	$PAI_{e_57.3}$
leaf-on coniferous scenes	0.92	1.39	1.97	1.64	1.64	1.54	1.75
leaf-on deciduous scenes	1.25	1.84	2.45	2.18	2.14	2.02	2.39
	$WAI_{e_Miller_10-65}$	$WAI_{e_Miller_0-80}$	$WAI_{e_Miller_0-90}$	$WAI_{e_LAI-2200}$	$WAI_{e_DHP_0-81}$	$WAI_{e_DHP_0-90}$	$WAI_{e_57.3}$
leaf-off deciduous scenes	0.46	0.70	0.87	0.83	0.83	0.79	0.93

For Miller_0-90, Figure 4 illustrates that the proportions of the number of scenes with null gap measurements to the total number of leaf-on deciduous and coniferous scenes at zenith angles in the 0–90° range are equal to zero if the zenith angles are <80°, and then they increased obviously at the zenith angles >80° and approach the maximum of 0.58 at the zenith angle of 88°. Compared with leaf-on forest scenes, the proportions of scenes with null gap measurements to the total number of leaf-off scenes at zenith angles in the 0–90° range are small; they are equal to zero if the zenith angle is <86° and approach the maximum of 0.09 at 87° (Figure 4). By contrast, for DHP_0-90, the proportions of the number of scenes with null gap measurements to the total number of leaf-on and leaf-off forest scenes at each annulus are always equal to zero.

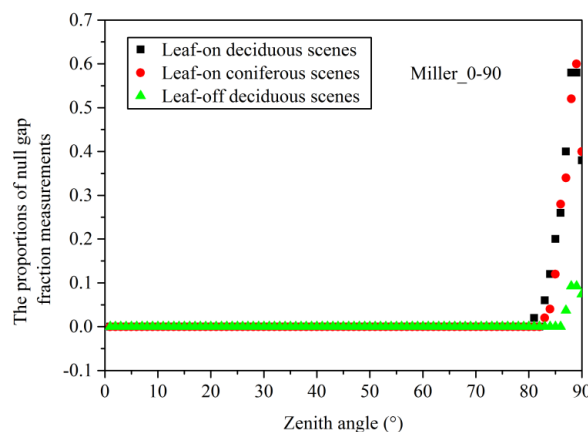


Figure 4. Proportions of number of scenes with null gap measurement at each zenith angle to the total number of leaf-on and leaf-off scenes for Miller_0-90.

4.1.2. G_e and G_w

The $G_e(\theta)$ of leaf-on coniferous scenes presents a trend similar to the planophile projection function, and they are decreased with zenith angles in the range of 0–90° (Figure 5). The $G_e(\theta)$ of leaf-on coniferous scenes is intersected with the line of $G_e(\theta) = 0.5$ at the zenith angle near 57.3° (Figure 5). In contrast, the $G_w(\theta)$ of leaf-off deciduous scenes exhibits a similar trend to the erectophile projection function, and they are increased with zenith angles in the range of 0–90° (Figure 5). The $G_w(\theta)$ of leaf-off deciduous scenes is intersected with the line of $G_w(\theta) = 0.5$ at the zenith angle near 52° (Figure 5). The $G_e(\theta)$ of leaf-on deciduous scenes exhibits a trend similar to spherical projection function, and the $G_e(\theta)$ is close to 0.5 at all the zenith angles ranging from 0° to 90° (Figure 5).

No significant differences were found between the mean PAI_e or WAI_e estimates of the seven inversion models (except Miller_10-65), which were estimated with or without consideration of G_e and G_w at all scenes, and the variations in proportion and differences are below 4% and 0.06, respectively (Tables 2 and 3). The variations in proportion and differences between the mean $PAI_{e_Miller_10-65}$ or $WAI_{e_Miller_10-65}$ estimated with or without consideration of G_e and G_w at all leaf-on and leaf-off scenes, are relatively large, ranging from 0–8% and 0–0.07, respectively (Tables 2 and 3). The variations in proportion and differences between the mean $PAI_{e_57.3}$ of leaf-on deciduous and coniferous scenes, which were derived with or without consideration of G_e , are 0% and 0.0, and 1% and 0.01, respectively; the variations in proportion and differences between the $WAI_{e_57.3}$ of leaf-off deciduous scenes, which were derived with or without consideration of G_w , are 3% and 0.03, respectively (Tables 2 and 3). The variations in proportion between the mean $PAI_{e_57.3}$ or $WAI_{e_57.3}$, which were derived with or without consideration of G_e and G_w at the leaf-on coniferous scenes and leaf-off deciduous scenes are not equal to zero due to the reason of the $G_e(\theta)$ of leaf-on coniferous scenes and the $G_w(\theta)$ of leaf-off deciduous scenes are not intersected with the lines of $G_e(\theta) = 0.5$ and $G_w(\theta) = 0.5$ at the zenith angle 57.3° (Figure 5).

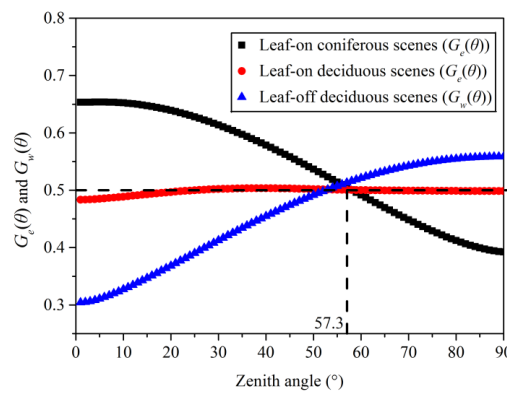


Figure 5. Mean $G_e(\theta)$ of all leaf-on coniferous and deciduous scenes and mean $G_w(\theta)$ of all leaf-off deciduous scenes.

Table 3. Mean PAI_e of leaf-on coniferous and deciduous scenes, and mean WAI_e of leaf-off deciduous scenes, which were estimated from the seven inversion models except Miller_0-90 using Equations (3)–(7), (9) and (10) considering G_e and G_w (γ_e , $\Omega_e(\theta)$, $\Omega_w(\theta)$, $\Omega_e(\theta')$, $\Omega_w(\theta')$, Ω_{e_i} and Ω_{w_i} are assumed to be equal to 1).

Inversion Model	Miller_10-65	Miller_0-80	LAI_2200	DHP_0-81	DHP_0-90	57.3
	$PAI_{e_Miller_10-65}$	$PAI_{e_Miller_0-80}$	$PAI_{e_LAI-2200}$	$PAI_{e_DHP_0-81}$	$PAI_{e_DHP_0-90}$	$PAI_{e_57.3}$
leaf-on coniferous scenes	0.85	1.39	1.59	1.70	1.59	1.74
leaf-on deciduous scenes	1.25	1.84	2.18	2.14	2.02	2.38
	$WAI_{e_Miller_10-65}$	$WAI_{e_Miller_0-80}$	$WAI_{e_LAI-2200}$	$WAI_{e_DHP_0-81}$	$WAI_{e_DHP_0-90}$	$WAI_{e_57.3}$
leaf-off deciduous scenes	0.49	0.71	0.86	0.83	0.80	0.90

4.1.3. γ_e , Ω_e , and Ω_w

This section focuses on the differences between the PAI_e or WAI_e , which were derived from the seven inversion models considering γ_e , Ω_e , or Ω_w , respectively. Evaluating the impact of different Ω_e and Ω_w estimation algorithms and segment sizes on the performance of the seven inversion models to estimate the PAI and WAI of leaf-on and leaf-off forest scenes is the target of the next section. For simplicity, only one segment size was analyzed in this section for LX and CLX.

Figure 6 shows that the mean $\Omega_e(\theta)$ and $\Omega_w(\theta)$ of all leaf-on and leaf-off scenes, which were derived from the four algorithms (CC, CLX, LX, and PCS), tended to increase and vary largely with zenith angles in the range of 10–90°, except the mean $\Omega_w(\theta)$ estimates derived from CLX_15 (hereafter, the 15 represent the segment size of 15° to derive Ω_e and Ω_w). Large differences were found between the four mean $\Omega_e(\theta)$ and $\Omega_w(\theta)$ estimates, which were estimated from the four Ω_e and Ω_w estimation algorithms at each zenith angle ranging from 10–90° at all leaf-on and leaf-off scenes (Figure 6). For example, for leaf-on deciduous scenes, the mean $\Omega_e(\theta)$, which were derived from CC at the four zenith angles of 10°, 30°, 60°, and 90° are 1.31, 1.46, 1.34, and 1.0 times the mean $\Omega_e(\theta)$ of CLX_15; 1.09, 1.05, 1.08, and 1.03 times the mean $\Omega_e(\theta)$ of LX_30; and 3.51, 3.73, 2.29, and 1.04 times the mean $\Omega_e(\theta)$ of PCS, respectively (Figure 6b).

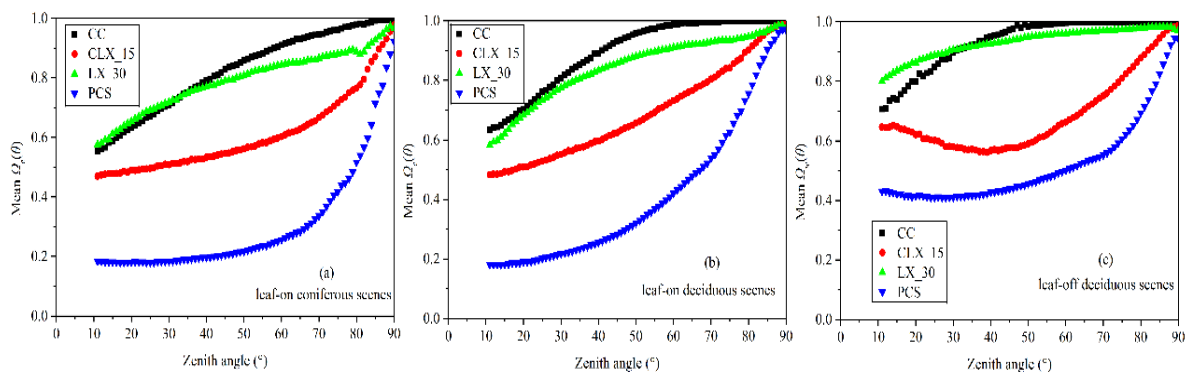


Figure 6. Mean $\Omega_e(\theta)$ and $\Omega_w(\theta)$ derived using CC, CLX_15, LX_30, and PCS at leaf-on coniferous scenes, (a) leaf-on deciduous scenes (b) and leaf-off deciduous scenes (c), respectively.

Compared with the differences between the mean PAI_e or WAI_e estimates of the seven inversion models, which were derived without consideration of γ_e , Ω_e , and Ω_w (Table 2), the differences between the PAI_e or WAI_e estimates of the seven inversion models, which were derived with consideration of γ_e , Ω_e , or Ω_w at the leaf-on and leaf-off scenes, tended to become larger (Table 4). The reason for the increase in the differences is that the PAI_e and WAI_e , which were derived considering γ_e , Ω_e , or Ω_w , were calculated by multiplying the PAI_e and WAI_e , which were estimated previously without consideration of γ_e , Ω_e , and Ω_w by the γ_e , $\frac{1}{\Omega_e(\theta)}$, or $\frac{1}{\Omega_w(\theta)}$, respectively. The values of γ_e , $\frac{1}{\Omega_e(\theta)}$, and $\frac{1}{\Omega_w(\theta)}$ are usually equal to or larger than unity for all leaf-on and leaf-off scenes (Figure 6 and Table 1). For example, for the leaf-on coniferous scenes, the difference between the $PAI_{e_Miller_10-65}$ and $PAI_{e_Miller_0-90}$ estimates, which was derived without consideration of γ_e and Ω_e is 1.05 (Table 1). This difference increased to 1.63 if γ_e was considered in the PAI_e estimation; similarly, the differences between the $PAI_{e_Miller_10-65}$ and $PAI_{e_Miller_0-90}$ estimates which were derived with consideration of Ω_e that were estimated using CC, CLX_15, LX_30, and PCS are increased to 1.08, 1.22, 1.12, and 1.79, respectively (Tables 2 and 4).

Table 4. Mean PAI_e of leaf-on coniferous and deciduous scenes and mean WAI_e of leaf-off deciduous scenes, which were derived from the seven inversion models using Equations (3)–(7), (9) and (10) considering γ_e , Ω_e , or Ω_w , respectively ($G_e(\theta)$ and $G_w(\theta)$ are assumed to be equal to 0.5). γ_e is assumed to be equal to 1.0 if Ω_e or Ω_w was considered in the PAI_e or WAI_e estimation. $\Omega_e(\theta)$, $\Omega_e(\theta')$, and Ω_{e_i} or $\Omega_w(\theta)$, $\Omega_w(\theta')$, and Ω_{w_i} are assumed to be equal to 1.0 if γ_e was considered in the PAI_e or WAI_e estimation.

Plant Function Types	Inversion Model	Miller_10-65	Miller_0-80	Miller_0-90	LAI_2200	DHP_0-81	DHP_0-90	57.3
		$PAI_{e_Miller_10-65}$	$PAI_{e_Miller_0-80}$	$PAI_{e_Miller_0-90}$	$PAI_{e_LAI-2200}$	$PAI_{e_DHP_0-81}$	$PAI_{e_DHP_0-90}$	$PAI_{e_57.3}$
Leaf-on coniferous scenes	Considering γ_e	1.42	2.14	3.05	2.52	2.52	2.37	2.68
	Considering Ω_e (CC)	1.04	1.53	2.12	1.83	1.78	1.68	1.82
	Considering Ω_e (CLX_15)	1.54	2.16	2.76	2.62	2.46	2.30	2.67
	Considering Ω_e (LX_30)	1.16	1.69	2.28	2.02	1.97	1.84	2.03
	Considering Ω_e (PCS)	3.77	4.90	5.56	6.11	5.34	5.0	6.29
Leaf-on deciduous scenes	Considering Ω_e (CC)	1.36	1.95	2.57	2.33	2.25	2.13	2.41
	Considering Ω_e (CLX_15)	1.88	2.58	3.22	3.15	2.91	2.76	3.18
	Considering Ω_e (LX_30)	1.50	2.15	2.74	2.54	2.44	2.34	2.62
	Considering Ω_e (PCS)	3.94	4.92	5.55	6.17	5.27	5.03	5.65
		$WAI_{e_Miller_10-65}$	$WAI_{e_Miller_0-80}$	$WAI_{e_Miller_0-90}$	$WAI_{e_LAI-2200}$	$WAI_{e_DHP_0-81}$	$WAI_{e_DHP_0-90}$	$WAI_{e_57.3}$
Leaf-off deciduous scenes	Considering Ω_w (CC)	0.48	0.71	0.89	0.85	0.85	0.81	0.93
	Considering Ω_w (CLX_15)	0.72	1.0	1.18	1.21	1.14	1.09	1.32
	Considering Ω_w (LX_30)	0.49	0.74	0.91	0.88	0.87	0.83	0.97
	Considering Ω_w (PCS)	0.97	1.35	1.54	1.65	1.53	1.44	1.80

Based on Tables 2 and 4, the changes between the variations in proportion between the PAI_e or WAI_e , which were derived from any two inversion models among the seven inversion models without consideration of Ω_e and Ω_w , and the variations in proportion between the PAI_e or WAI_e derived from the same two inversion models with consideration of Ω_e and Ω_w , are correlated to the Ω_e and Ω_w estimation algorithms. Minor or no changes were observed in the differences of proportion between the PAI_e or WAI_e , which were derived from any two inversion models among the seven inversion models without consideration of Ω_e and Ω_w , and the differences in proportion between the PAI_e or WAI_e , which were derived from the same two inversion models considering Ω_e and Ω_w , which were estimated using CC and LX_30 (<6%, <7%, and <2% at the leaf-on deciduous, leaf-on coniferous, and leaf-off deciduous scenes, respectively). The differences in proportion between the PAI_e or WAI_e derived from any two inversion models among the seven inversion models considering Ω_e and Ω_w , which were estimated using CLX_15 and PCS, are smaller about 1–22%, 0–29%, and 0–11% than those between the PAI_e or WAI_e , which were derived from the same two inversion models without consideration of Ω_e and Ω_w at the leaf-on deciduous, leaf-on coniferous, and leaf-on deciduous scenes, respectively. No changes were observed in the variations in proportion between the PAI_e derived from any two inversion models among the seven inversion models without consideration of γ_e at leaf-on coniferous scenes, and the variations in proportion between the PAI_e derived from the same two inversion models with consideration of γ_e .

4.2. Estimation of the PAI_e , PAI , PAI_e and WAI of Leaf-on and Leaf-off Forest Scenes from the Seven Inversion Models

4.2.1. Leaf-on Forest Scenes

All the seven inversion models except Miller_0-90 tended to underestimate the PAI of leaf-on scenes if γ_e and Ω_e were not considered in the PAI estimation (Figure 7). The PAI_e estimates derived from the seven inversion models without consideration of γ_e and Ω_e were 5–103% of the true PAI of the leaf-on forest scenes (Figure 7). Most of the PAI_e estimates derived from Miller_0-90 and 57.3 were 35–75% of the true PAI of leaf-on forest scenes (Figure 7c,g). From the root mean square error (RMSE), mean absolute error (MAE), and the regression slope, Miller_0-90 performed the best with the smallest RMSE and MAE as compared with the other inversion models for estimating the PAI_e of leaf-on forest scenes, followed by 57.3 and DHP_0-81 (Figure 7e,g). The worst results were obtained with Miller_10-65 with the largest RMSE and MAE (Figure 7a).

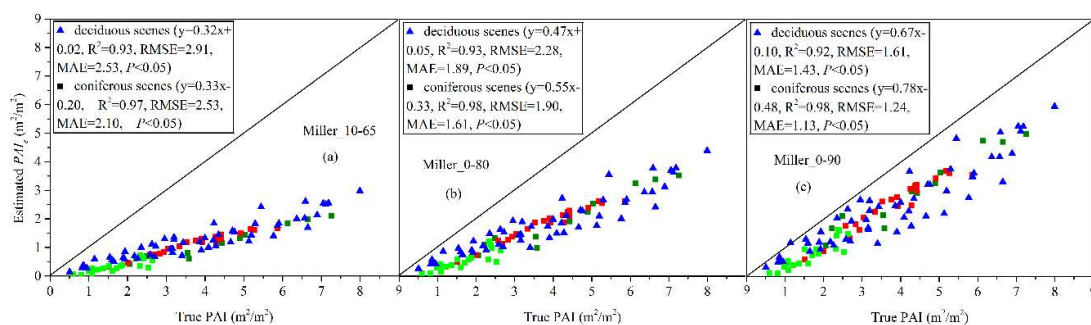


Figure 7. Cont.

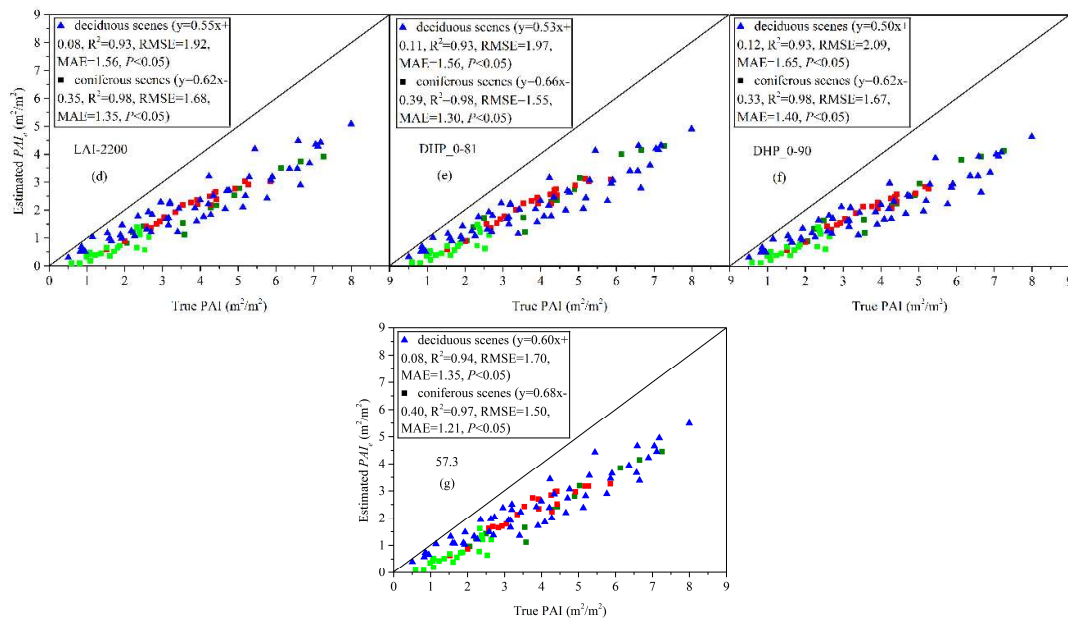


Figure 7. Comparison of true PAI of leaf-on coniferous and deciduous scenes with PAI_e estimates derived from the seven inversion models without consideration of γ_e and Ω_e : (a) Miller_10-65 ($PAI_{e_Miller_10-65}$), (b) Miller_0-80 ($PAI_{e_Miller_0-80}$), (c) Miller_0-90 ($PAI_{e_Miller_0-90}$), (d) LAI-2200 ($PAI_{e_LAI-2200}$), (e) DHP_0-81 ($PAI_{e_DHP_0-81}$), (f) DHP_0-90 ($PAI_{e_DHP_0-90}$), and (g) 57.3 ($PAI_{e_57.3}$). The PAI_e estimates were derived from the seven inversion models using Equations (3)–(7), (9) and (10) with consideration of G_e (γ_e , $\Omega_e(\theta)$, $\Omega_e(\theta')$, and Ω_{e_i} are assumed to be equal to 1). Statistics are given at 95% confidence level from two-tailed Student's t -test. Olive square: SPS, red square: JPSS, green square: OPSW.

The performance of the seven inversion models in estimating the PAI of leaf-on coniferous and deciduous scenes was largely improved if the γ_e and Ω_e were considered in the PAI estimation, except the combinations of the inversion models, γ_e , Ω_e estimation algorithm, and segment size with PCS (Figures 7–9). For leaf-on coniferous and deciduous scenes, the PAI, which was estimated from the seven inversion models considering γ_e and Ω_e , was closer to the one-to-one line compared with the PAI_e estimated from the same inversion model without consideration of γ_e and Ω_e , except the combination of inversion model, γ_e , Ω_e estimation algorithm, and segment size with PCS (Figures 7–9). For example, for leaf-on deciduous scenes, clear evidence of the improvement in the PAI estimation was provided by the fact that the RMSE, MAE, and regression slope of the PAI_e estimates, which were estimated from Miller_0-90 without consideration of γ_e and Ω_e , were 1.61, 1.43, and 0.67; they decreased to 0.83, 0.54, and 0.82 when γ_e and LX_5 were considered in the PAI estimation (Figure 7 and Table A1).

The best performance of the combination of inversion model, γ_e , Ω_e estimation algorithm, and segment size to estimate the PAI of leaf-on coniferous and deciduous scenes is the function of plant functional types (Figures 8 and 9, Table A1). Furthermore, the best combination of inversion model, γ_e , Ω_e estimation algorithm, and segment size to estimate the PAI of the leaf-on coniferous scenes is also different at the two sub-series coniferous scenes of JPSS and OPSW and SPS (Figure 8 and Table A1). Based on the RMSE, MAE, and regression slope, the combination of Miller_0-90 and LX_5 performed the best to estimate the PAI of leaf-on deciduous scenes, followed by the combinations of 57.3 and LX_5, LAI-2200 and LX_5, and Miller_0-90 and CLX_15, respectively (Figure 9 and Table A1). Amongst the combinations of inversion model, γ_e , Ω_e estimation algorithm, and segment size tested, DHP_0-90 and LX_5 performed the best, followed by DHP_0-81 and CLX_45, DHP_0-81, and CLX_30, and LAI-2200 and CLX_45 for estimating the PAI of sub-series coniferous scenes of JPSS and OPSW (Figure 8 and Table A1). The combination of inversion model, γ_e , Ω_e estimation algorithm, and segment size with Miller_0-80 and CC exhibited the best performance in estimating the PAI of SPS coniferous

scenes, followed by Miller_0-80 and LX_30, Miller_0-80 and CLX_45, and LAI-2200 and CC (Figure 8 and Table A1).

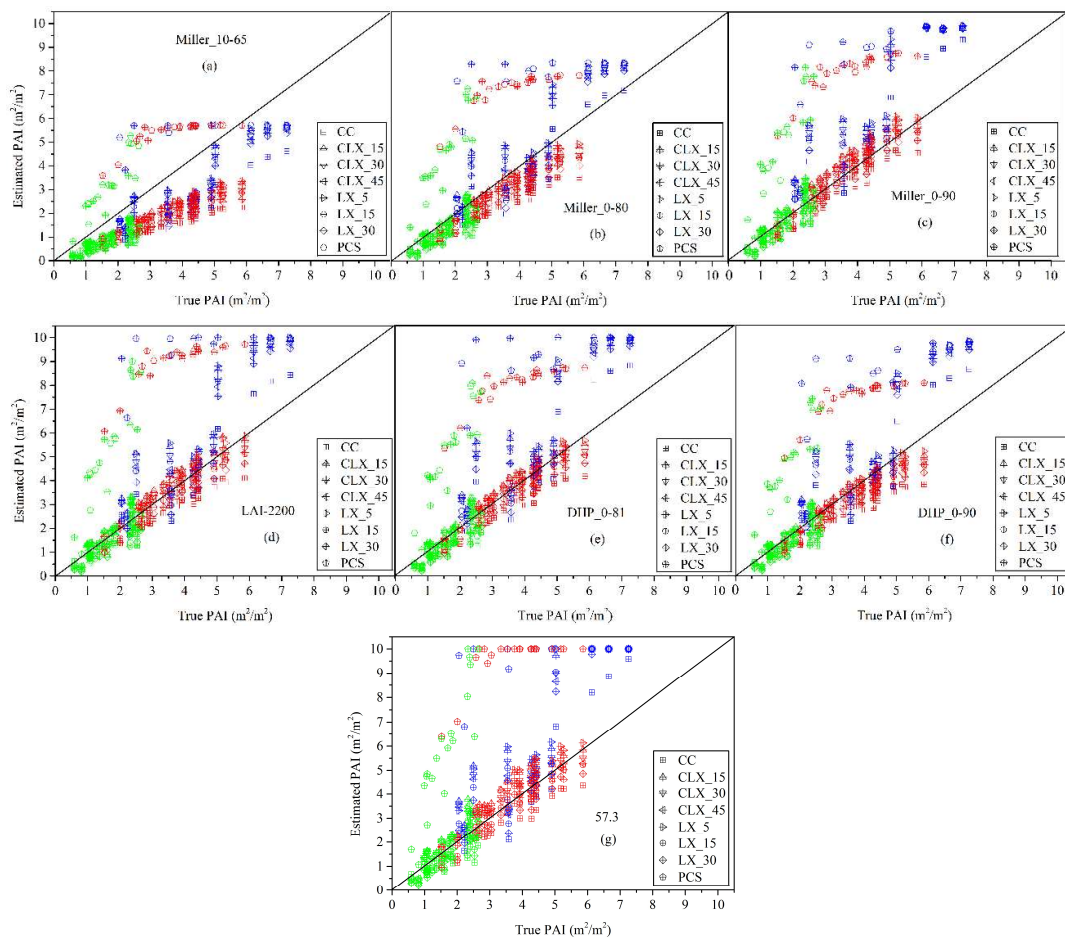


Figure 8. (a–g) Comparison of true PAI of leaf-on coniferous forest scenes with PAI calculated from the seven inversion models with consideration of G_e , γ_e , and Ω_e . Four Ω_e estimation algorithms (CC, LX, CLX, and PCS) were used to estimate the Ω_e of leaf-on coniferous scenes. Blue: SPS, red: JPSS, green: OPSW.

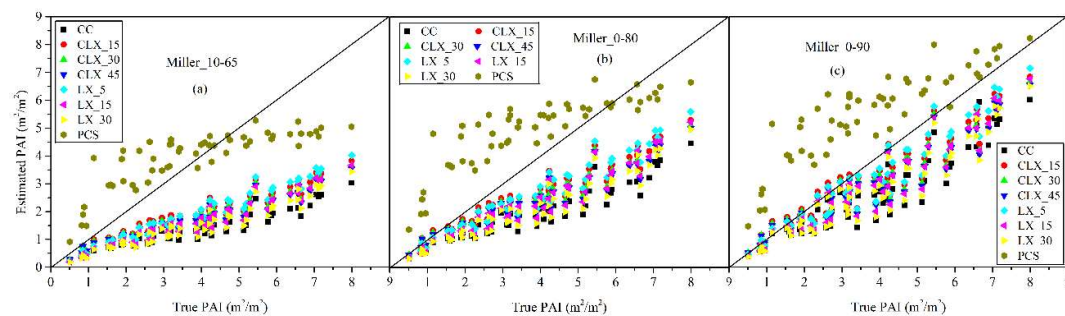


Figure 9. Cont.

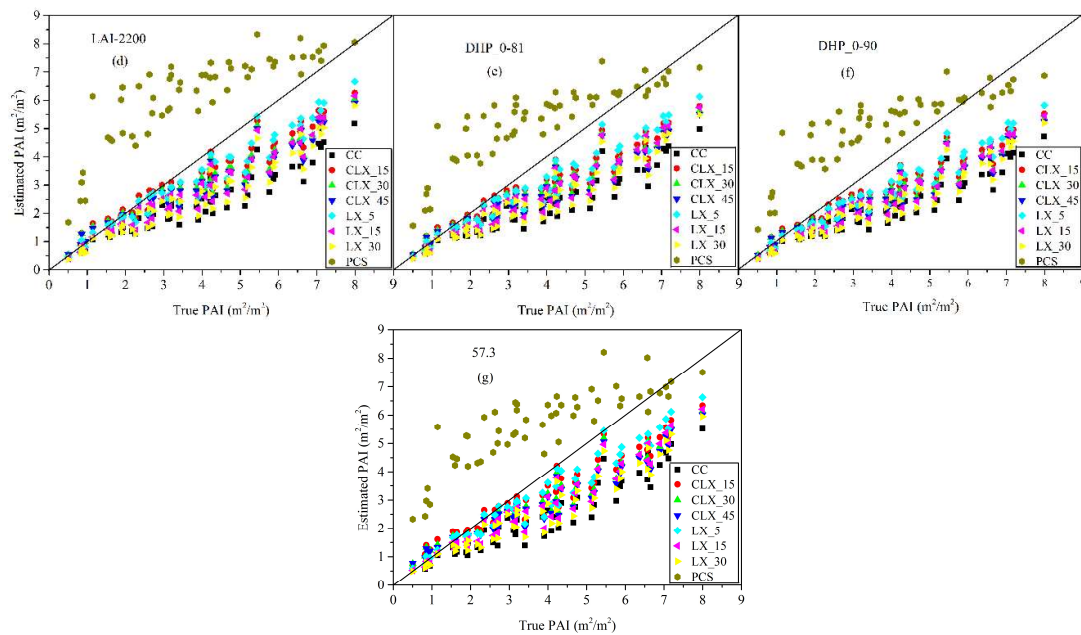


Figure 9. (a–g) Comparison of true PAI of leaf-on deciduous forest scenes with PAI calculated from the seven inversion models with consideration of G_e and Ω_e . Four Ω_e estimation algorithms (CC, LX, CLX, and PCS) were used to estimate the Ω_e of leaf-on deciduous scenes.

4.2.2. Leaf-off Forest Scenes

All the seven inversion models tended to underestimate the WAI at the majority of leaf-off scenes if Ω_w was not considered in the WAI estimation (Figure 10). The WAI_e estimates derived from the seven inversion models are 28–126% of the true WAI of leaf-off deciduous scenes (Figure 10). Most of the WAI_e estimates derived from Miller_0-90 and 57.3 were 63–90% of the true WAI of leaf-off deciduous forest scenes (Figure 10c,g). Based on RMSE, MAE, and regression slope, the 57.3 inversion model performed the best amongst the seven inversion models to estimate the WAI_e of leaf-off deciduous forest scenes with the smallest RMSE and MAE, followed by Miller_0-90 and LAI-2200 (Figure 10d,g). The worst results were obtained with Miller_10-65 with the largest RMSE and MAE compared with other inversion models (Figure 10a).

The underestimation of the seven inversion models to estimate the WAI of leaf-off deciduous scenes without consideration of Ω_w was significantly reduced if Ω_w was considered in the WAI estimation, except the combinations of inversion model, Ω_w estimation algorithm and segment size with PCS (Figures 10 and 11, Table A2). For example, the RMSE, MAE, and regression slope of the WAI estimated from 57.3 without consideration of Ω_w were 0.30, 0.18, and 0.76, respectively, which decreased to 0.16, 0.06, and 0.89 for the WAI estimated from 57.3 with consideration of LX_5 (Figures 10 and 11, Table A2). Based on the RMSE, MAE, and regression slope, the combination of inversion model, Ω_w estimation algorithm, and segment size of LAI-2200 and LX_5 performed the best in estimating the WAI of leaf-off deciduous scenes, followed by the combinations of 57.3 and LX_5, DHP_0-81 and LX_5, and Miller_0-90 and LX_5 (Table A2).

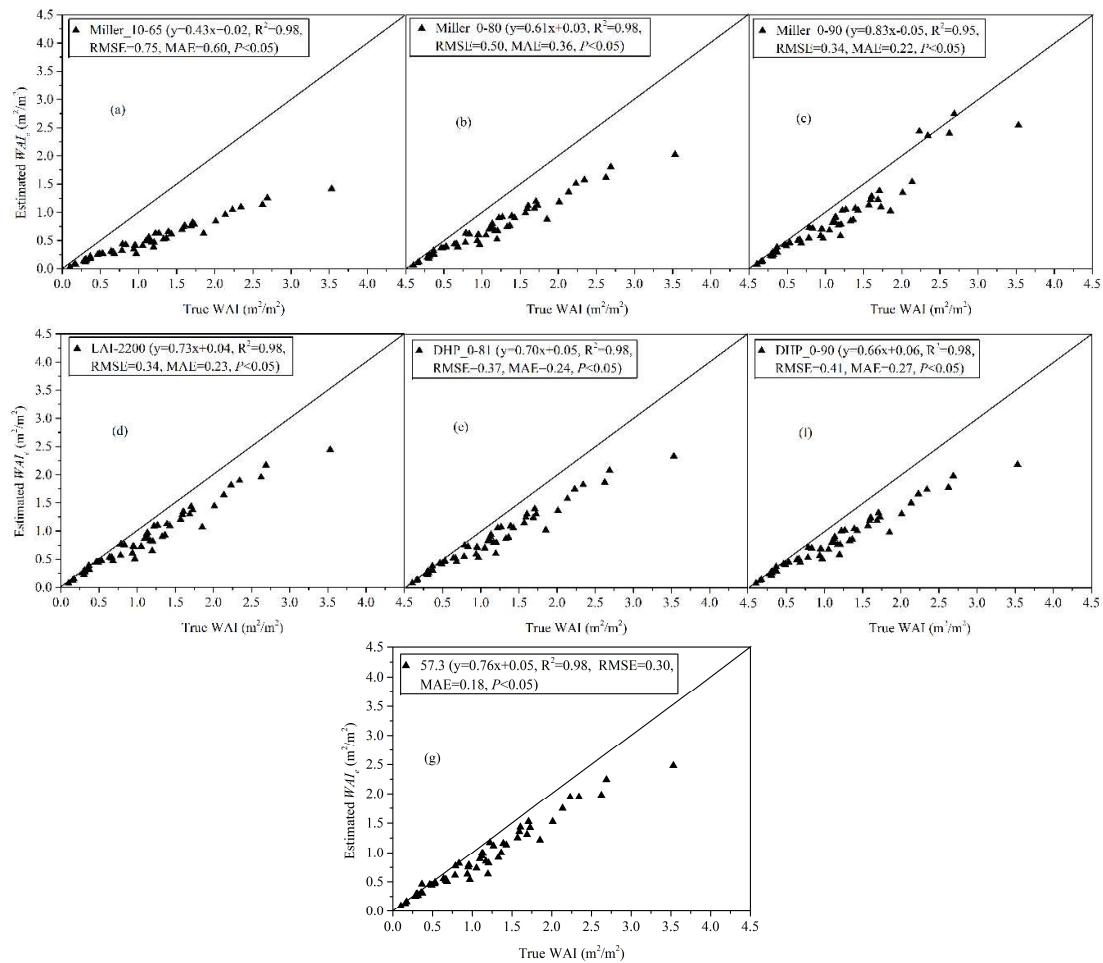


Figure 10. Comparison of true WAI of leaf-off deciduous forest scenes with WAI_e estimates derived from seven inversion models without considering Ω_w : (a) Miller_10-65 ($WAI_{e_Miller_10-65}$), (b) Miller_0-80 ($WAI_{e_Miller_0-80}$), (c) Miller_0-90 ($WAI_{e_Miller_0-90}$), (d) LAI-2200 ($WAI_{e_LAI-2200}$), (e) DHP_0-81 ($WAI_{e_DHP_0-81}$), (f) DHP_0-90 ($WAI_{e_DHP_0-90}$), and (g) 57.3 ($WAI_{e_57.3}$). The WAI_e estimates were estimated using Equations (3)–(7), (9) and (10) with consideration of G_w (γ_e , $\Omega_w(\theta)$, $\Omega_w(\theta')$, and Ω_{w_i} are assumed to be equal to 1). Statistics are given at 95% confidence level from two-tailed Student’s *t*-test.

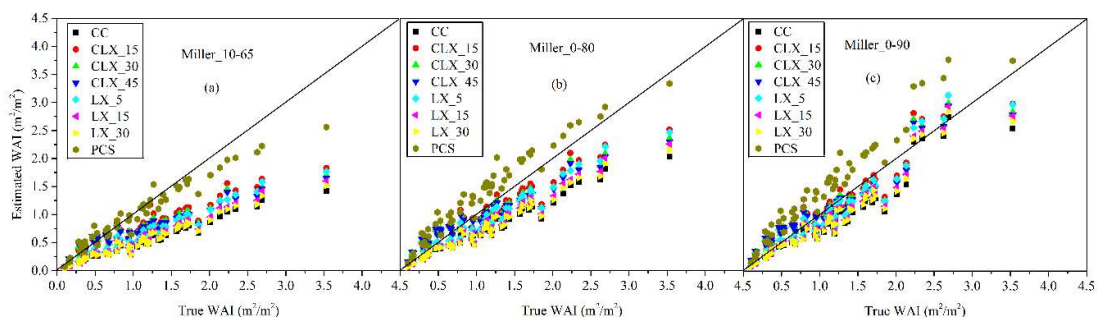


Figure 11. Cont.

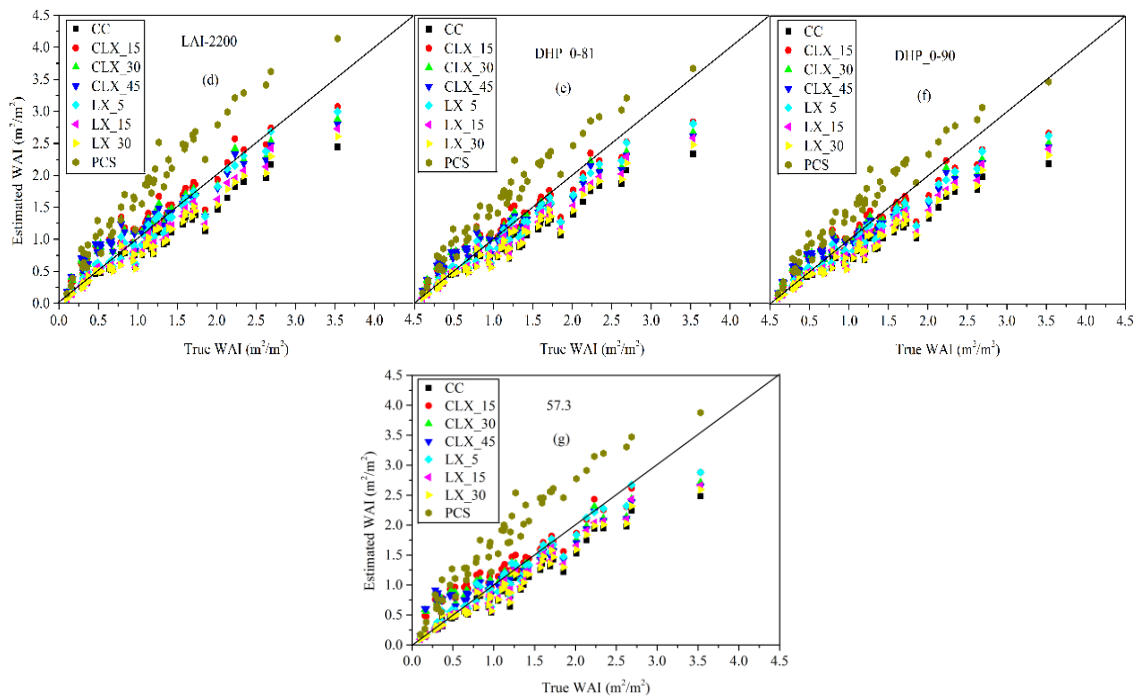


Figure 11. (a–g) Comparison of true WAI of leaf-off deciduous forest scenes with WAI calculated from the seven inversion models with consideration of G_w and Ω_w . Four Ω_w estimation algorithms (CC, LX, CLX, and PCS) were used to estimate the Ω_w of leaf-off deciduous scenes.

5. Discussion

The main finding of our study is that no universally valid combination of inversion model, γ_e , Ω_e and Ω_w estimation algorithm, and segment size is available to obtain accurate estimates of PAI and WAI for all leaf-on and leaf-off forest canopies. Both the factors of inversion model, G_e , G_w , γ_e , Ω_e , Ω_w , and segment size are contributed to the differences between the PAI and WAI estimated from the seven inversion models. The performance of the combination of inversion model, γ_e , Ω_e and Ω_w , estimation algorithm, and segment size to estimate the PAI and WAI of leaf-on and leaf-off forest scenes is the function of the inversion model, γ_e , Ω_e and Ω_w estimation algorithm, segment size, PAI, WAI, tree species composition, and plant functional types.

5.1. Reason for Differences between PAI_e , PAI, WAI_e and WAI Estimates Estimated from the Seven Inversion Models with or without Consideration of G_e , G_w , γ_e , Ω_e , and Ω_w

Since $p_e(\theta)$, $p_w(\theta)$, $G_e(\theta)$, $G_w(\theta)$, $\Omega_e(\theta)$, and $\Omega_w(\theta)$ varied obviously with zenith angles in the range of 0–90° (Figures 3, 5 and 6). The trend in the variations of $G_e(\theta)$, $G_w(\theta)$, $\Omega_e(\theta)$, and $\Omega_w(\theta)$ with zenith angles in the range of 0–90° did not comply with the trend in the variations of $p_e(\theta)$ and $p_w(\theta)$ in the same zenith angle range (Figures 3, 5 and 6). However, different zenith angle ranges were used by the seven inversion models to estimate the PAI and WAI of leaf-on and leaf-off forest scenes. Therefore, both the inversion model, G_e , G_w , γ_e , Ω_e and Ω_w estimation algorithm, and segment size are the factors that contributed to the differences between the PAI or WAI estimated from the seven inversion models. That's because the $p_e(\theta)$, $p_w(\theta)$, $p_{e_i}(\theta_i)$, $p_e(\theta')$, $p_w(\theta')$, $p_{e_i}(\theta_i)$, $p_{w_i}(\theta_i)$, $G_e(\theta)$, $G_w(\theta)$, G_{e_i} , G_{w_i} , $\Omega_e(\theta)$, $\Omega_w(\theta)$, Ω_{e_i} , and Ω_{w_i} that were used in the PAI and WAI estimation for the seven inversion models are obviously different between each other.

Amongst the five factors of the inversion model, G_e and G_w , γ_e , Ω_e and Ω_w estimation algorithm, and segment size, the PAI and WAI estimation was less affected by G_e and G_w ; by contrast, the PAI and WAI estimation was largely affected by other factors (Figures 8, 9 and 11, Tables 2–4, A1 and A2) (Appendix C.1). The largest variation in proportion between the PAI_e , PAI, WAI_e , and WAI estimated

from any two inversion models amongst the seven inversion models with or without consideration of γ_e , G_e , G_w , Ω_e , and Ω_w at the leaf-on and leaf-off scenes is that derived from Miller_10-65 and Miller_0-90 (Equations (3) and (5)) without consideration of γ_e , Ω_e , and Ω_w , but with consideration of G_e and G_w (Figures 8, 9 and 11, Tables 2–4, A1 and A2). The mean PAI_e and WAI_e estimates derived from Miller_0-90 are approximately two times the estimates derived from Miller_10-65 (Table 2). This result means that the inversion model contributed more to the variations between the results of the seven inversion models as the variations in proportion tended to decrease if Ω_e and Ω_w were considered in the PAI_e , PAI, WAI_e , and WAI estimation (Tables 2, 4, A1 and A2). The zenith angle ranges covered by the two inversion models of Miller_10-65 and Miller_0-90 and the processing solution of the null gap fraction measurements can explain the large differences between the mean PAI_e or WAI_e estimates of the two inversion models. The reason is that both the logarithm of the mean $p_e(\theta)$ and $p_w(\theta)$, and the weight ($\sin(\theta)d\theta$) tended to increase with zenith angles in the range of 0–90° (Figure 3). Further, the defined PAI and WAI of 10 for the null gap fraction measurements at the zenith angles close to the horizon are usually larger than the estimates derived using Equation (4) based on the mean $p_e(\theta)$ and $p_w(\theta)$ collected at the zenith angle range of 10–65°.

Compared with two inversion models, namely, Miller_10-65, and Miller_0-90, the variations in proportion between the mean PAI_e or WAI_e estimates of any other two inversion models estimated without consideration of Ω_e and Ω_w are relatively small (Tables 2–4). The variations of the $\Omega_e(\theta)$ and $\Omega_w(\theta)$ in the zenith angle range of 0–90° at the leaf-on and leaf-off forest canopy are specific to sites, species, and estimation algorithms [10,17,41,61]. Chen et al. [61] reported that the Ω_e of most natural forest stands range from 0.50 to 0.75. Similarly, the γ_e of the coniferous forest canopy is also specific to sites and tree species, and previous studies reported that γ_e usually ranges from 1.20 to 2.08 [10,22,47]. Therefore, amongst the four factors of the inversion model, γ_e , Ω_e and Ω_w estimation algorithm, and segment size, the dominant factor that contributed more to the differences between the PAI or WAI estimated from the seven inversion models except Miller_10-65 considering γ_e , G_e , G_w , Ω_e , and Ω_w is the function of the inversion model, γ_e , Ω_e and Ω_w estimation algorithm, segment size, and tree species composition, and the structural characteristics of the forest canopy.

The differences between the mean PAI_e or WAI_e results of the two inversion models covered with the same zenith angle ranges, such as Miller_0-90 and DHP_0-90, and DHP_0-81 and DHP_0-90, are mainly deduced from the differences between the gap fraction and weight calculation methods of the two inversion models (Tables 2 and 3). For these inversion models covered with different zenith angle ranges, such as Miller_0-80 and Miller_0-90, and Miller_0-80 and DHP_0-90, all the three aspects of the inversion model, including zenith angle range, gap fraction, and weight calculation methods, are the main sources of differences between the PAI_e or WAI_e estimates of the different inversion models (Figure 4, Tables 2 and 3).

5.2. Can PAI or WAI be Estimated Accurately from the Currently Available Inversion Models without Field Measurements of $G_e(\theta)$ and $G_w(\theta)$ of Forest Canopy

To address the challenge of measuring the $G_e(\theta)$ and $G_w(\theta)$ of the leaf-on and leaf-off forest canopy, the 57.3 inversion model was recommended by many previous studies to derive the PAI and LAI of vegetation canopy [18,22,45,62]. Previous studies showed that this inversion model is a good choice to avoid the error source of G_e and G_w in the PAI and WAI estimation of vegetation canopy [18,45,62]; this conclusion was also confirmed in the present study (Figure 5 and Tables 2 and 3). The merit of the 57.3 inversion model is that the $G_e(\theta)$ and $G_w(\theta)$ of leaf-on and leaf-off forest canopy were approximately intersected at the zenith angle near 57.3° (1 radian) and are equal to about 0.5 at this zenith angle [7,15,45,63]; this conclusion was also confirmed in the present study at the leaf-on and leaf-off scenes with three typical and contrasting types of G_e and G_w (Figure 5).

Since the $G_e(\theta)$ and $G_w(\theta)$ varied obviously with zenith angles in the range of 0–90° (Figure 5), the $G_e(\theta)$ and $G_w(\theta)$ measurements would be the critical input parameters for the seven inversion models except 57.3 in the PAI and WAI estimation of leaf-on and leaf-off scenes. A sign of

the important role of G_e and G_w in the PAI and WAI estimation is that large differences were found between the PAI_e or WAI_e estimates derived from Miller_10-65 estimated with or without consideration of G_e and G_w (Tables 2 and 3). The large differences indicate that it is inappropriate to assume that $G_e(\theta)$ and $G_w(\theta)$ are equal to 0.5 at all zenith angles in the PAI and WAI estimation. However, the minor differences in proportion between the PAI_e or WAI_e estimated using the inversion models of Miller_0-80, LAI-2200, DHP_0-81, and DHP_0-90 with or without consideration of G_e and G_w are small (below <4%) (Tables 2 and 3), showing that the error source of G_e and G_w was largely reduced in the PAI_e and WAI_e estimation. The zenith angle ranges covered by the four inversion models is the reason for the reduction of the error source of G_e and G_w in the PAI_e and WAI_e estimation. As inferred from Equation (4) that the PAI and WAI are linearly related to the $G_e(\theta)$ and $G_w(\theta)$, respectively, therefore, the PAI and WAI estimation errors are equivalent in proportion to the G_e and G_w errors. Therefore, the trade-off between the PAI_e and WAI_e overestimation or underestimation caused by the underestimation or overestimation of $G_e(\theta)$ and $G_w(\theta)$ at zenith angles less than near 57° , and the opposite trend of the PAI_e and WAI_e underestimation or overestimation caused by the overestimation or underestimation of $G_e(\theta)$ and $G_w(\theta)$ at zenith angles greater than near 57° are the reason for the removal of the error source of $G_e(\theta)$ and $G_w(\theta)$ in the PAI_e and WAI_e estimation for the four inversion models (Figure 5, Tables 2 and 3). The larger values of the logarithm of the mean $p_e(\theta)$ and $p_w(\theta)$, and $\sin(\theta)d\theta$ at the zenith angle range of $57-90^\circ$ compared with those at the zenith angle range of $0-57^\circ$ can explain why a narrow zenith angle range of the former zenith angle range is enough to trade off the PAI_e and WAI_e underestimation or overestimation caused by the error source of $G_e(\theta)$ and $G_w(\theta)$ at the latter zenith angle range. Therefore, we can conclude that the impact of G_e and G_w on the PAI_e , WAI_e , PAI, and WAI estimation of leaf-on and leaf-off forest canopy can be reduced to a low level (4%) by selecting appropriate inversion models such as Miller_0-80, LAI-2200, DHP_0-81, DHP_0-90, and 57.3.

5.3. Can the Ω_e and Ω_w of Leaf-on and Leaf-off Forest Canopy be Effectively Estimated based on the DHP Images Using the Currently Available Algorithms

The PAI and WAI underestimation of the seven inversion models were largely reduced or removed if the γ_e , Ω_e , and Ω_w were considered in the PAI and WAI estimation of leaf-on and leaf-off scenes, except the combinations of inversion model, γ_e , Ω_e , and Ω_w estimation algorithm and segment size with PCS (Figures 7–11, Tables A1 and A2). Therefore, we can conclude that the clumping effect of the canopy element and woody component of the forest canopy was the main reason for the severe PAI and WAI underestimation of the seven inversion models if γ_e , Ω_e , and Ω_w were not considered in the PAI and WAI estimation. This finding is consistent with the conclusions drawn from previous studies which reported that the large underestimation of PAI for optical methods are due to the clumping effect of the canopy element of the forest canopy [15,18,34,35,56]. However, Leblanc and Fournier [18] reported an opposite conclusion that the WAI estimated using the 57.3 inversion model without consideration of Ω_w were close to the true WAI of leaf-off forest scenes. The WAI corrected by Ω_w were found to be larger than the true WAI of leaf-off forest scenes in their study [18]. The nature of the 3D tree models of leaf-off forest scenes used in their study compared with those in the present study is the factor that contributed to the different conclusions drawn in these two studies. The leaf-off tree models represented by trunks only (without branches) were adopted by Leblanc and Fournier [18], but the leaf-off detailed 3D tree models with trunks and branches were used in the present study to generate the leaf-off forest scenes. The diameters of trunks are larger than those of branches, and trunks are closer to the sensor compared with the branches in the upper canopies, making the trunks contribute more gap fraction measurements as they would. The branches contribute 50–70% of the WAI of the forest canopy [64]; the absence of branches in leaf-off forest scenes would further increase the clumping effect of the woody component, resulting in the overestimation of WAI corrected by Ω_w in the study by Leblanc and Fournier [18].

The distinct PAI underestimation for all the combinations of inversion model, γ_e , Ω_e estimation algorithm, and segment size except those with PCS at the leaf-on deciduous scenes with PAI > ~3.5 (Figure 9), indicating that the Ω_e of those scenes was not accurately estimated by the three algorithms of CC, LX, and CLX. Cutini et al. [32] reported that the leaves of deciduous forest canopy tended to concentrate at the top crown to compete for light. Therefore, limited direct sunlight can penetrate through the top crown of these forest canopies and into the ground for those with large PAI. Furthermore, insufficient gap fraction or gap size measurements that the Ω_e estimation algorithms rely on to estimate Ω_e were collected from these leaf-on deciduous forest canopies would cause the Ω_e estimation algorithms to underestimate Ω_e . Thus, the Ω_e underestimation would be the main reason for the overall PAI underestimation at the leaf-on deciduous forest canopy with relatively large PAI. For leaf-on deciduous forest scenes, if the inversion models are the same, the combinations of inversion model, γ_e , Ω_e estimation algorithm, and segment size with LX_5 performed the best, followed by the combinations with CLX_15 in the PAI estimation, except the combinations with Miller_10-65. This conclusion does not contradict the finding of Woodgate [45] even though different tree species were examined in these two studies. Woodgate reported that CLX_15 performed the best compared with other combinations of Ω_e estimation algorithm (CC, LX, and CLX) and segment size (15°, 45°, and 90°) to estimate the Ω_e of eucalypt forest canopy, but LX_5 was not analyzed in that study [45]. Better performance of LX to estimate the Ω_e of leaf-on *Gliricidia sepium* forest canopy was also reported by van Gardingen et al. [25]; they found that the PAI underestimation decreased from 50% to 15% after the PAI estimates were corrected by Ω_e derived using LX.

Compared with the leaf-on deciduous forest scenes, the gap fraction or gap size measurements collected at leaf-off deciduous forest scenes would be relatively sufficient as leaves were removed from the canopy and only woody components were left. Therefore, the accuracy of the Ω_w estimates estimated from CC, CLX, and LX at leaf-off deciduous forest scenes would be improved compared with those estimated at the leaf-on deciduous forest scenes. A sign of the improvement of the accuracy of the Ω_w estimates at the leaf-off deciduous forest scenes is that the WAI estimated from all combinations of inversion model, Ω_w estimation algorithm, and segment size at the leaf-off deciduous scenes were closer to the one-to-one line compared with the PAI estimated using the same combination of the inversion model, γ_e , Ω_e estimation algorithm, and segment size at the leaf-on deciduous scenes (Figures 9 and 11). The large slope and small RMSE and MAE of the combinations of inversion model, Ω_w estimation algorithm, and segment size with LX_5 except those combinations with Miller_10-65 and Miller_0-80 indicating that the Ω_w of leaf-off deciduous scenes can be accurately estimated if appropriate Ω_w estimation algorithm and segment size was adopted (Table A2).

The PAI estimated from the seven inversion models except Miller_10-65 at the leaf-on coniferous forest canopy are close to the one-to-one line, except at the sub-series coniferous scenes of SPS (Figure 8). This result indicates that the Ω_e of the sub-series coniferous scenes of JPSS and OPSW was accurately estimated by CLX if appropriate segment size was adopted. Furthermore, accurate PAI estimates can be obtained at the sub-series coniferous scenes of JPSS and OPSW if γ_e and Ω_e were considered in the PAI estimation (Figure 8 and Table A1). For the sub-series coniferous scenes of SPS, the PAI estimated from all the combinations of inversion model, γ_e , Ω_e estimation algorithm, and segment size at six scenes deviated largely from the one-to-one line, regardless of the inversion model, Ω_e estimation algorithm, and segment size used by the combinations, except those combinations with Miller_10-65 (Figure 8). Upon further examination, the reference Ω_e of the six scenes range from 1.0 to 1.35. The stem distribution mode of five of the six scenes is regular. Currently, the Ω_e estimation algorithms except PCS used in this study cannot effectively deal with the situations of regular distribution of the canopy element in space at the scale of beyond-shoot. The Ω_e estimation algorithms would overestimate $\Omega_e(\theta)$ in the six scenes with reference $\Omega_e \geq 1.0$, as the $\Omega_e(\theta)$ estimates obtained from these Ω_e estimation algorithms were always ≤ 1 (Appendix C.3). Therefore, the $\Omega_e(\theta)$ overestimation would be the reason for the severe PAI overestimation at the six scenes of the sub-series coniferous scenes of SPS. If the six scenes with reference $\Omega_e \geq 1$ were removed from the sub-series coniferous scenes of SPS, then the

combinations of inversion model, γ_e , Ω_e estimation algorithm, and segment size with LX_15 would perform the best followed by combinations with the same inversion model but with CLX to estimate the PAI of the sub-series coniferous scenes of SPS, except combinations with Miller_10-65, Miller_0-80, and Miller_0-90. This finding is different from the conclusion of Pisek et al. [60], who reported that CLX outperformed other Ω_e algorithms (CC, LX, and CMN) to estimate the Ω_e of an old Scots Pine plot with the age of 124 years. The one plot covered in the study of Pisek et al. [60] and only six scenes of the sub-series coniferous scenes of SPS left after removing those SPS scenes with reference $\Omega_e \geq 1$ may have contributed to the differences between the conclusions drawn from these two studies.

In conclusion, the best performance of Ω_e and Ω_w estimation algorithms in estimating the Ω_e and Ω_w of leaf-on and leaf-off forest canopy is the function of tree species and plant functional types. The different characteristics of the clumping effect of canopy element and woody component between the leaf-on deciduous scenes, leaf-on coniferous scenes, and leaf-off deciduous scenes and the obvious differences between the $\Omega_e(\theta)$ and $\Omega_w(\theta)$ estimates derived from the four Ω_e and Ω_w estimation algorithms (CC, CLX, LX, and PCS) with different theoretical basis have contributed to the different conclusions of the best combination of Ω_e and Ω_w estimation algorithm and segment size to estimate the Ω_e and Ω_w of the leaf-on and leaf-off scenes (Figures 6, 8, 9 and 11, Tables A1 and A2). No universally valid Ω_e and Ω_w estimation algorithm and segment size is available to accurately estimate the Ω_e and Ω_w of all leaf-on and leaf-off scenes, respectively. This finding indicates that there is still room to improve the performance of the currently available Ω_e and Ω_w estimation instruments and algorithms to accurately estimate the Ω_e and Ω_w of leaf-on and leaf-off forest canopy, especially for those canopies with reference Ω_e and $\Omega_w > 1$ (Appendix C.3).

There are several critical problems still existed for the four Ω_e and Ω_w estimation algorithms. For example, segment size is a key parameter for LX and CLX to estimate the Ω_e and Ω_w of leaf-on and leaf-off forest canopy. However, determining appropriate segment sizes of LX and CLX is difficult, particularly for the DHP approach [18,26,45]. Gonsamo et al. [26] reported that the Ω_e estimates derived from LX decreased evidently by decreasing segment sizes from 15° to 5° and slightly changed further by decreasing segment sizes from 5° to 2.5°. The minor variations in the Ω_e estimates obtained from LX using the latter range of segment sizes indicate that the spatial distribution of the canopy element in all segments was approaching the assumption of random distribution. Improved accuracy of Ω_e estimates obtained from LX with smaller segment sizes was reported by previous studies [26,45]. This trend was also observed in the present study (Tables A1 and A2). However, the proportions of segments without gaps in all the segments also increased dramatically if small segment sizes were used to estimate Ω_e and Ω_w [18,26,45]. The logarithm of the gap fraction of these segments without gaps gave undefined results, and a subjectively assumed PAI or WAI is typically assigned to these segments [17,26]. Therefore, the assumed PAI or WAI for the segments without gaps would be an error source for LX. On the other hand, the lack of ability of LX to recognize and utilize large gaps of between-crown clumping to estimate the Ω_e and Ω_w of leaf-on and leaf-off forest canopy remains unresolved, regardless of segment size ranging from large (120°) to small (5° or 2.5°).

Besides the two disadvantages of LX described, there are two more problems related to the small segment size faced for CLX. Firstly, the short length of segment increases the possibility of null gaps or full gaps in the transect of segment as reported previously [18,26,45]. Secondly, the short length of segment will likely violate the assumption of an infinite horizontal plane defined by the CC algorithm [58]. However, CC relies on the collected gap size measurements to evaluate the clumping effect of the canopy element and woody component at the segment scale. Therefore, the limited and insufficient gap sizes collected by CLX at the transect of each segment compared with TRAC would become the weakness of CLX in evaluating the clumping effect of the canopy element and woody component at the segment scale. The combinations of the inversion model, γ_e , Ω_e and Ω_w estimation algorithm, and segment size with CLX did not always perform better than other combinations with the same inversion models but with different Ω_e and Ω_w estimation algorithms to estimate the PAI and WAI of leaf-on and leaf-off scenes (Figures 8, 9 and 11, Tables A1 and A2). This finding is not consistent

with the conclusions of Gonsamo and Pellikka [41], Leblanc and Fourier [18], and Woodgate [45] that CLX is better than other Ω_e estimation algorithms (CC, LX, and PCS) in estimating the Ω_e of the leaf-on forest canopy. Both the plant functional types, 3D forest scenes and segment sizes contributed to the differences between the conclusions drawn in the present and previous studies. The RMSE and MAE of the PAI and WAI estimated from the combination of inversion model, γ_e , Ω_e and Ω_w estimation algorithm, and segment size with LX_5 at the leaf-on and leaf-off deciduous scenes were smaller than those estimated from the combinations with the same inversion model but with CLX (Table A1), illustrating that the clumping effect of the canopy element and woody component at the segment scale was not thoroughly measured by CC for CLX.

For PCS, the significant PAI and WAI overestimation for the combination of the inversion model, γ_e , Ω_e , and Ω_w algorithm and segment size with PCS illustrated that PCS overestimated the Ω_e and Ω_w remarkably at both the leaf-on and leaf-off scenes (Figures 8, 9 and 11). The Ω_e and Ω_w overestimation for PCS was also reported in previous studies [41,43]. The combinations of the inversion model, γ_e , Ω_e , and Ω_w estimation algorithm and segment size with CC underestimated the PAI and WAI of leaf-on and leaf-off forest scenes, except at the SPS coniferous scenes (Figures 8, 9 and 11). This finding is consistent with the reports of Pisek et al. [60], Leblanc and Fourier [18], and Woodgate [45] that parts of the large nonrandom gaps were not removed by CC, leading to an underestimation of Ω_e and Ω_w , and underestimated the PAI and WAI of forest canopy further.

Because the performance of the seven inversion models to estimate the PAI and WAI of the leaf-on and leaf-off forest canopy with consideration of γ_e , Ω_e , and Ω_w were strongly dependent on the accuracies of the Ω_e and Ω_w estimates (Tables A1 and A2) (Appendix C.1). All the above-mentioned problems of the four Ω_e and Ω_w algorithms (CC, CLX, LX, and PCS) need to be solved reasonably in the future to improve the accuracies of the Ω_e and Ω_w estimates derived from the four algorithms.

5.4. Which Inversion Model(s) is (are) More Reliable to Estimate the PAI and WAI of the Leaf-on and Leaf-off Forest Canopy

The zenith angle ranges covered by the seven inversion models are apparently different. As explained previously, the zenith angle range covered by Miller_10-65 is the reason why the PAI and WAI estimated from the combination of the inversion model, γ_e , Ω_e and Ω_w estimation algorithm, and segment size with Miller_10-65 were still smaller than those estimated from other combinations with different inversion models but with the same Ω_e and Ω_w estimation algorithm and segment size. On the other hand, the PAI and WAI underestimation of Miller_10-65 illustrates the necessity of incorporating the gap fraction measurements at large zenith angles, which were not covered by Miller_10-65, to the PAI and WAI estimation of the leaf-on and leaf-off forest canopy. However, a problem in using the gap fraction measurements at large zenith angles in the PAI and WAI estimation is the high probability of obtaining null gap fraction measurements at these zenith angles, as reported by previous studies [17,25,26] and the present study (Figure 4). Several solutions were proposed to address the undefined inversion of the null gap fraction measurements, such as adding half or one pixel to the annulus of the DHP images or defining arbitrary upper PAI or LAI limit values of 8 or 10 [17,25,26]. However, those proposed solutions cannot derive accurate PAI and LAI estimates for those annuli without gaps due to evident subjectivities. Therefore, the processing solutions of the null gap fraction measurements would produce estimation errors to the derived PAI and WAI estimates. Significant differences were observed between $PAI_{e_Miller_0-90}$ and $PAI_{e_DHP_0-90}$ or $WAI_{e_Miller_0-90}$ and $WAI_{e_DHP_0-90}$ estimates at the leaf-on and leaf-off scenes, respectively, especially for those scenes with $PAI_{e_} > 2.5$ at the leaf-on scenes and $WAI_{e_} > 2.25$ at the leaf-off scenes (Figure 7c,f and Figure 10c,f) (Appendix C.2). The significant differences indicate that the PAI_e and WAI_e estimation were largely affected by the processing solutions of the null gap fraction measurements as the null gap fraction measurements at the zenith angles close to the horizon were completely removed for DHP_0-90 at all annuli compared with Miller_0-90 (Figure 4), and the same zenith angle range of 0–90° was covered by the two inversion models. Similarly, the PAI and WAI estimation errors of the processing solutions of

the null gap fraction measurements can also be avoided for the two inversion models of LAI-2200 and DHP_0-81 as the same zenith angle width of annulus of 10° was adopted by the two inversion models to obtain the gap fraction measurements similar to DHP_0-90.

Compared with six other inversion models, the 57.3 inversion model shows three advantages in estimating the PAI and WAI of the leaf-on and leaf-off forest canopy. Firstly, the 57.3 inversion model is simple to apply. Furthermore, the $G_e(\theta)$ and $G_w(\theta)$ of leaf-on and leaf-off forest canopy can be assumed to be equal to approximately 0.5 at the zenith angle of 57.3° . Thus, no $G_e(\theta)$ and $G_w(\theta)$ measurements need to be collected in the field if the 57.3 inversion model would be used to estimate the PAI and WAI of forest canopy. Secondly, determining the exposure settings for imaging DHP photographs that can avoid overexposure near the zenith and underexposure near the horizon is difficult in the field. Accurate exposure settings to collect DHP images can be obtained due to the reason that only the gap fraction measurements with zenith angles near 57.3° are needed for the 57.3 inversion model. Thirdly, determining a reasonable threshold to binarize all the pixels of DHP images with zenith angles ranging from 0° to 90° is difficult because light conditions change across different image areas of the DHP images. Therefore, an accurate threshold that is used to binarize the DHP images can be obtained if only the pixels with zenith angles near 57.3° were considered for the PAI and WAI estimation. The 57.3 inversion model does not always outperform other inversion models to estimate the PAI and WAI of all leaf-on and leaf-off forest canopies although it can provide PAI and WAI estimates with relatively good accuracies compared with other inversion models if appropriate Ω_e and Ω_w estimation algorithms would be adopted, and the Ω_e , γ_e , and Ω_w would be considered in the PAI and WAI estimation (Figures 8, 9 and 11 and Appendix C.1). With the merits of the 57.3 inversion model described, the 57.3 inversion model can be treated as an alternative choice to estimate the PAI and WAI of the leaf-on and leaf-off forest canopy if the best combination of inversion model, γ_e , Ω_e and Ω_w estimation algorithm, and segment size remains unknown.

In conclusion, based on Figures 8, 9 and 11, Tables A1 and A2, we suggest that 57.3, LAI-2200, and Miller_0-90 followed by DHP_0-81, DHP_0-90, and Miller_0-80 to be used in estimating the PAI and WAI of the leaf-on and leaf-off forest canopy. The PAI and WAI estimated from Miller_0-90 were closer to the one-to-one line compared with those derived from DHP_0-90, although the impact of the null gap fraction measurements of each zenith angle on the PAI and WAI estimation was difficult to evaluate quantitatively in the field, caution is needed if Miller_90 would be used to estimate the PAI and WAI of the leaf-on and leaf-off forest canopy, especially for canopies with large PAI and WAI.

The performance of the seven inversion models to estimate the PAI and WAI of the leaf-on and leaf-off forest canopy with consideration of γ_e , Ω_e , and Ω_w was significantly affected by the Ω_e and Ω_w estimation algorithm and segment size used, and also the true PAI and WAI, and the reference Ω_e and Ω_w of leaf-on and leaf-off forest scenes (Appendix C). Therefore, the performance of the inversion model to estimate the PAI and WAI of the leaf-on and leaf-off forest canopy is the function of Ω_e and Ω_w estimation algorithm, segment size, reference Ω_e and Ω_w , PAI, WAI, and plant functional types. No universal best inversion model is available to estimate the PAI and WAI of all the leaf-on and leaf-off forest canopies even if γ_e , Ω_e , and Ω_w were considered in the PAI and WAI estimation.

5.5. Limitations and Perspectives

If Miller_0-90 (Equation (3)) would be adopted to estimate the PAI_e and WAI_e of the leaf-on and leaf-off forest scenes based on the mean $p_e(\theta)$ and $p_w(\theta)$ at zenith angles in the $0-90^\circ$ range with interval of 1° (Figure 3), then the proportions of the PAI_e and WAI_e measurements derived at the zenith angle range of $0-9^\circ$ to the PAI_e and WAI_e , which were estimated using Miller_0-90 (Equation (3)) at the full zenith angle range of $0-90^\circ$, are both below 1% at the leaf-on and leaf-off scenes. This result indicates that the estimation error is small when we assume that the $\Omega_e(\theta)$ and $\Omega_w(\theta)$ estimates with zenith angles in the $0-9^\circ$ range with interval of 1° are equal to the $\Omega_e(\theta)$ and $\Omega_w(\theta)$ at the zenith angle of 10° in the PAI and WAI estimation of the five inversion models of Miller_0-80, Miller_0-90, LAI-2200, DHP_0-81, and DHP_0-90 in this study. An option to cope with the defect of the assumption

made in this study is to estimate the $\Omega_e(\theta)$ and $\Omega_w(\theta)$ of the leaf-on and leaf-off forest canopy at the zenith angle range of 0–9° using TRAC, multispectral canopy imager (MCI) [8], and digital cover photography (DCP) [24] at the zenith angles ranging from 0–9°.

A dataset of field measurements of the PAI and WAI of leaf-on and leaf-off forest canopy would be useful to understand the performance of the seven inversion models in estimating the PAI and WAI when the field plots cover a wider range of PAI, WAI, Ω_e , Ω_w , γ_e , tree species composition, and plant functional types. The ground slope would also influence the seven inversion models to estimate the PAI and WAI of the leaf-on and leaf-off forest canopy and can be evaluated in the future.

6. Conclusions

The conclusions of this study are as follows: (1) Both the factors of inversion model, canopy element and woody component projection functions, canopy element and woody component estimation algorithms, and segment size are contributed to the differences between the PAI and WAI estimated from the seven inversion models. (2) No universally valid combination of inversion model, γ_e , Ω_e and Ω_w , estimation algorithm, and segment size is available to obtain accurate estimates of PAI and WAI for all leaf-on and leaf-off forest canopies. The best combination of inversion model, γ_e , Ω_e and Ω_w estimation algorithm, and segment size to estimate the PAI and WAI of leaf-on and leaf-off forest scenes is the function of inversion model, γ_e , Ω_e and Ω_w estimation algorithm, segment size, tree species composition, and plant functional types. (3) The impact of G_e and G_w measurements on the PAI and WAI estimation of the leaf-on and leaf-off forest canopy can be reduced to a low level (<4%) and neglected in the PAI and WAI estimation by adopting appropriate inversion models. Accurate PAI and WAI of forest canopy can be estimated from the DHP method without the field measurements of $G_e(\theta)$ and $G_w(\theta)$. (4) We suggest 57.3, LAI-2200, and Miller_0-90 followed by DHP_0-81, DHP_0-90, and Miller_0-80 to be used in estimating the PAI and WAI of the leaf-on and leaf-off forest canopy. Caution is needed if Miller_90 would be used to estimate the PAI and WAI of the leaf-on and leaf-off forest canopy, especially for canopies with large PAI and WAI. (5) The performance of the combinations of inversion model, γ_e , Ω_e and Ω_w estimation algorithm, and segment size to estimate the PAI and WAI of leaf-on and leaf-off forest canopy strongly relied on the accuracies of the Ω_e and Ω_w estimates. LX and CLX performed better than the two other algorithms in estimating the Ω_e and Ω_w of the leaf-on and leaf-off forest canopy, respectively. However, the best combinations of the Ω_e and Ω_w estimation algorithm, and segment size to estimate the Ω_e and Ω_w of the leaf-on and leaf-off forest canopy depend on the plant functional types and tree species composition. Caution is needed in applying the conclusions of this study to estimate the PAI and WAI of forest canopy with different tree species compositions or plant function types.

Author Contributions: J.Z. designed the framework of ILMSVP, proposed the concept of this study, analyzed the data, and wrote the paper. Y.Z., F.C., and S.L. wrote the paper. C.M., W.L., and P.L. developed and ran the ILMSVP software. B.Y. analyzed the data.

Funding: This work was jointly funded by the Open Fund of State Key Laboratory of Remote Sensing Science (Grant No. OFSLRSS201721), the National Natural Science Foundation of China (Grant Nos. 41371330, 41001203), the Project of Excellent Young Scientists of Fujian Province (Grant No. JA14033), and the Program for New Century Excellent Talents in Fujian province.

Conflicts of Interest: The authors declare no conflicts of interest.

Appendix A. List of Symbols

- 57.3 the 57.3 inversion model (Equation (4))
- $A(\theta, \theta_e)$ the projection coefficient at the canopy element inclination angle of θ_e and the view zenith angle of θ
- CC the gap size distribution algorithm
- CLX the combination of gap size and logarithmic averaging algorithm
- CMN the modified gap size distribution algorithm

- DBH diameter at breast height
- DCP digital cover photography
- DHP digital hemispherical photography
- DHP_0-81 the DHP_0-81 inversion model (Equation (9))
- DHP_0-90 the DHP_0-90 inversion model (Equation (10))
- $f(\theta_e)$ canopy element angle distribution function
- $f(\theta_w)$ woody component angle distribution function, θ_w is the woody component inclination angle
- G_e canopy element projection function
- G_w woody component projection function
- $G_e(\theta)$ the mean projection of unit surface area of the canopy element on the plane perpendicular to the view zenith angle of θ
- $G_w(\theta)$ the mean projection of unit surface area of the woody component on the plane perpendicular to the view zenith angle of θ
- G_{e_i} the G_e estimate of the i th annulus
- G_{w_i} the G_w estimate of the i th annulus
- ILMSPV In situ LAI Measurements Simulation and Validation Platform software
- JBSS Järvelja birch stand (summer)
- JBSW Järvelja birch stand (winter)
- JPSS Järvelja pine stand (summer)
- LAI leaf area index
- LAI-2200 the LAI-2200 inversion model (Equation (7))
- LUT look-up table
- LX the logarithmic averaging algorithm
- LXW the modified logarithmic averaging algorithm
- MAE mean absolute error
- MCI multispectral canopy imager
- Miller_0-90 the Miller theorem (Equation (3))
- Miller_10-65 the Miller_10-65 inversion model (Equation (5))
- Miller_0-80 the Miller_0-80 inversion model (Equation (6))
- MTVSP the measurement tools of vegetation structural parameters software
- OPSW Ofenpass pine stand (winter)
- PAI plant area index
- PAI_e effective plant area index
- $PAI_{e_Miller_0-90}$ effective plant area index estimated from Equation (3) with the assumption that γ_e or $\Omega_e(\theta)$ is equal to 1
- $PAI_{e_57.3}$ effective plant area index estimated from Equation (4) with the assumption that γ_e or $\Omega_e(\theta')$ is equal to 1
- $PAI_{e_Miller_10-65}$ effective plant area index estimated from Equation (5) with the assumption that γ_e or $\Omega_e(\theta)$ is equal to 1
- $PAI_{e_Miller_0-80}$ effective plant area index estimated from Equation (6) with the assumption that γ_e or $\Omega_e(\theta)$ is equal to 1
- $PAI_{e_LAI-2200}$ effective plant area index estimated from Equation (7) with the assumption that γ_e or Ω_{e_i} is equal to 1
- $PAI_{e_DHP_0-81}$ effective plant area index estimated from Equation (9) with the assumption that γ_e or Ω_{e_i} is equal to 1
- $PAI_{e_DHP_0-90}$ effective plant area index estimated from Equation (10) with the assumption that γ_e or Ω_{e_i} is equal to 1

- PCS the Pielou's coefficient of spatial segregation algorithm
- $p_e(\theta)$ canopy element gap fraction at θ
- $p_{e_i}(\theta_i)$ the canopy element gap fraction of the i th annulus at θ
- R^2 pearson correlation coefficient
- RMSE the root mean square error
- SPS Scots pine scenes
- TRAC tracing radiation and architecture of canopies
- WAI woody area index
- WAI_e effective woody area index
- $WAI_{e_Miller_0-90}$ effective woody area index estimated from Equation (3) with the assumption that $\Omega_w(\theta)$ is equal to 1
- $WAI_{e_57.3}$ effective woody area index estimated from Equation (4) with the assumption that $\Omega_w(\theta')$ is equal to 1
- $WAI_{e_Miller_10-65}$ effective woody area index estimated from Equation (5) with the assumption that $\Omega_w(\theta)$ is equal to 1
- $WAI_{e_Miller_0-80}$ effective woody area index estimated from Equation (6) with the assumption that $\Omega_w(\theta)$ is equal to 1
- $WAI_{e_LAI-2200}$ effective woody area index estimated from Equation (7) with the assumption that Ω_{w_i} is equal to 1
- $WAI_{e_DHP_0-81}$ effective woody area index estimated from Equation (9) with the assumption that Ω_{w_i} is equal to 1
- $WAI_{e_DHP_0-90}$ effective woody area index estimated from Equation (10) with the assumption that Ω_{w_i} is equal to 1
- W_i the weight factor of the i th annulus
- θ zenith angle
- θ_i the center zenith angle of the i th annulus
- θ' the single zenith angle (or centered at an angle for a range of angles) of the PAI estimation
- Ω_e canopy element clumping index
- Ω_w woody component clumping index
- $\Omega_e(\theta)$ canopy element clumping index at θ
- $\Omega_w(\theta)$ woody component clumping index at θ
- Ω_{e_i} the Ω_e estimate of the i th annulus
- Ω_{w_i} the Ω_w estimate of the i th annulus
- γ_e needle-to-shoot area ratio

Appendix B. In Situ LAI Measurements Simulation and Validation Platform (ILMSVP)

ILMSVP provides the ability of generating forest scenes based on the 3D tree models and the input parameters of stand density, tree stem distribution mode, and scene size. The forest scenes were generated in accordance with the following rules: (i) The voxel-based tree models with the voxel element size of $0.1 \text{ m} \times 0.1 \text{ m} \times 0.1 \text{ m}$ were produced for all explicit 3D tree models one by one. The total voxel number of each tree model was calculated based on the height, width, and depth of the minimum bounding box of the tree model. For each tree model, the attribute of 1 was assigned to those voxels, within which any canopy elements are located, otherwise, 0 was assigned to other voxels. (ii) If the stand density of the scene is smaller than the designated parameter, then a tree model was randomly chosen from all the candidate tree models and randomly placed in the scene. Newly placed tree models in the scenes were tested to check if they overlapped with existing surrounding trees within the 3D space before they were placed in the scenes. If the voxels with the attribute of 1 of the newly placed tree models overlapped with any voxels with the attribute of 1 of other tree models, then the

newly placed tree models were either rotated with a specified azimuth angle to avoid overlapping or moved to a new location. (iii) All trees in the scenes (100 m × 100 m) were placed following a customized tree stem distribution pattern, such as random, regular, and clumped. The spatial locations of the tree models of those scenes with clumped stem distribution mode were calculated using the deformation-kernel method proposed by Brendan and Przemyslaw [65]. (iv) All the scenes with size of 900 m × 900 m were reproduced using a scene-cloning technique. Firstly, a small scene with size of 100 m × 100 m was created through the aforementioned two steps. Then, four scenes were cloned in four orthogonal directions adjacent to the small scene. The other forest scenes (100 m × 100 m) within the scenes with size of 900 m × 900 m were cloned in a similar manner using a different centric scene each time. To improve the randomness of the scenes, all the cloned scenes were rotated with a random azimuthal angle of 0°, 90°, 180°, and 270° before planting.

Reverse ray-tracing method was previously used to generate the black-and-white binary DHP images within the forest scenes [18,41,42]. This method was also adopted by ILMSPV to generate the binary DHP images within the central area of each scene with the size of 25 m × 25 m. A perfect fisheye lens (with 180° field of view) with polar projection was chosen to generate DHP images. The resolution of the generated DHP images was 4000 pixels × 4000 pixels, and the camera height was 1.0 m. For every pixel in the generated images, a single ray was traced from the camera position in the direction of the pixel centroid to determine if there was an intersection event between the ray and canopy element [45]. The ray tracing would result in preclassified binary images of black (0, intersected; canopy element) and white pixels (1, passed or not intersected; sky). For simplicity, the DHP images were assumed to be generated under ideal uniform sky conditions. Majasalmi et al. [66] and Nackaerts et al. [67] reported that a sampling scheme with 12 to 15 randomly distributed sampling points would be enough to obtain the accurate gap fraction measurements of the forest canopy. A cross-pattern sampling scheme comprising 13 sampling points (5 m separation excluding central sampling point), of which 4 are located near the center with a distance of 5 m between one another, was adopted by ILMSPV as the sampling scheme to arrange the sampling points at the central area of each scene. This cross-sampling scheme was also used by Leblanc and Fournier [18] to obtain the Ω_e and Ω_w of the leaf-on and leaf-off forest canopy based on DHP method.

Appendix C. Factors that Affect the Performance of the Seven Inversion Models to Estimate the PAI and WAI of Leaf-on and Leaf-off Forest Scenes

Appendix C.1. Inversion Model, Ω_e and Ω_w , Estimation Algorithm, and Segment Size

Appendix C.1.1. Leaf-on Forest Scenes

Large differences were observed between the PAI derived from the combinations of inversion model, γ_e , Ω_e estimation algorithm, and segment size with different inversion models but with the same Ω_e estimation algorithm and segment size, and from the combinations with the same inversion model but with different Ω_e estimation algorithms and segment sizes, and from the combinations with the same inversion model and Ω_e estimation algorithm but with different segment sizes (Figures 8 and 9, Table A1). For example, Figure 9d shows large differences between the PAI estimated from the three combinations of LAI-2200 and CC, LAI-2200 and LX_5 and LAI-2200 and PCS at the leaf-on deciduous scenes (Table A1). Another evidence of the significant differences between the PAI estimates of the three combinations are the large differences between the RMSE, MAE and regression slope of the three combinations, which are 1.79, 1.33, 0.54; 0.89, 0.57, 0.75; and 2.60, 2.50, 0.64, respectively (Table A1). Similarly, the RMSE, MAE and regression slope of the two combinations of LAI-2200 and LX_15 and LAI-2200 and LX_30 are 1.28, 0.96, 0.68, and 1.52, 1.19, 0.63, respectively (Table A1). The large differences between the RMSE, MAE, and regression slope of the two groups of the three combinations of inversion model, γ_e , Ω_e estimation algorithm, and segment size indicate that the performance of the seven inversion models to estimate the PAI of leaf-on coniferous and deciduous scenes with consideration of γ_e and Ω_e are strongly dependent on the Ω_e estimation algorithm and

segment size used. The RMSE, MAE, and regression slope of the PAI, which were estimated from the three combinations of Miller_10-65 and LX_5, Miller_0-90, and LX_5, and DHP_0-90 and LX_5 at the sub-series coniferous scenes of JPSS and OPSW, are 2.22, 1.87, 0.46; 0.83, 0.54, 0.82, and 1.29, 0.85, 0.65, respectively (Table A1). The large difference between the RMSE, MAE, and regression slope of the three combinations illustrate that the inversion model also plays a key role to influence the performance of the combination of inversion model, γ_e , Ω_e estimation algorithm, and segment size to estimate the PAI of leaf-on deciduous and coniferous scenes (Figures 8 and 9, Table A1).

The combinations of inversion model, γ_e , Ω_e estimation algorithm, and segment size with CLX and LX, and CC and LX performed better than the combinations with the same inversion model but with different Ω_e estimation algorithms to estimate the PAI of the two sub-series coniferous scenes of JPSS and OPSW and another sub-series coniferous scenes of SPS, respectively, except those combinations with Miller_10-65 and Miller_0-80 (Figure 8 and Table A1). For leaf-on deciduous scenes, the combinations of inversion model, γ_e , Ω_e estimation algorithm, and segment size with LX and CLX performed better than the combinations with the same inversion model but with two other estimation algorithms to estimate the PAI, except the combinations with Miller_10-65 (Figure 9 and Table A1).

Table A1. Correlation statistics between true and estimated PAI calculated from seven inversion models with consideration of G_e , γ_e , and Ω_e at three groups of sub-series scenes. RMSE and MAE are expressed in PAI units (m^2/m^2).

Inversion Models	PAI Estimation	Sub-Series Scenes	R^2	Intercept	Slope	RMSE	MAE
Miller_10-65	Considering γ_e and Ω_e (CC)	JPSS, OPSW	0.98	0.05	0.40	1.80	1.53
		SPS	0.93	-0.62	0.70	2.05	2.19
		JBSS	0.95	0.14	0.32	2.83	2.40
	Considering γ_e and Ω_e (CLX_15)	JPSS, OPSW	0.98	-0.01	0.62	1.20	0.96
		SPS	0.93	-0.24	0.84	1.10	0.90
		JBSS	0.97	0.34	0.40	2.27	1.82
	Considering γ_e and Ω_e (CLX_30)	JPSS, OPSW	0.98	0.07	0.56	1.31	1.05
		SPS	0.93	-0.33	0.83	1.24	1.0
		JBSS	0.96	0.34	0.38	2.39	1.92
	Considering γ_e and Ω_e (CLX_45)	JPSS, OPSW	0.97	0.11	0.53	1.37	1.10
		SPS	0.93	-0.41	0.82	1.35	1.18
		JBSS	0.96	0.34	0.36	2.46	2.0
	Considering γ_e and Ω_e (LX_5)	JPSS, OPSW	0.98	-0.21	0.67	1.23	1.01
		SPS	0.93	-0.34	0.87	1.08	0.89
		JBSS	0.98	0.14	0.46	2.22	1.87
	Considering γ_e and Ω_e (LX_15)	JPSS, OPSW	0.98	-0.21	0.57	1.52	1.34
		SPS	0.93	-0.77	0.89	1.39	1.09
		JBSS	0.97	0.07	0.41	2.50	2.08
	Considering γ_e and Ω_e (LX_30)	JPSS, OPSW	0.98	-0.20	0.52	1.68	1.49
		SPS	0.93	-0.92	0.87	1.61	1.33
		JBSS	0.96	0.05	0.37	2.66	2.21
	Considering γ_e and Ω_e (PCS)	JPSS, OPSW	0.86	1.57	0.97	1.69	1.37
		SPS	0.54	4.73	0.17	1.80	1.48
		JBSS	0.81	2.39	0.41	1.30	0.89
Miller_0-80	Considering γ_e and Ω_e (CC)	JPSS, OPSW	0.98	-0.03	0.66	1.09	0.97
		SPS	0.92	-0.83	1.10	0.89	0.59
		JBSS	0.94	0.19	0.46	2.18	1.73
	Considering γ_e and Ω_e (CLX_15)	JPSS, OPSW	0.98	0.05	0.90	0.39	0.21
		SPS	0.91	0.12	1.17	1.27	0.88
		JBSS	0.96	0.46	0.56	1.55	1.04
	Considering γ_e and Ω_e (CLX_30)	JPSS, OPSW	0.98	0.11	0.83	0.49	0.31
		SPS	0.91	-0.12	1.18	1.13	0.78
		JBSS	0.96	0.44	0.53	1.68	1.16
	Considering γ_e and Ω_e (CLX_45)	JPSS, OPSW	0.98	0.14	0.79	0.57	0.40
		SPS	0.92	-0.30	1.18	1.02	0.67
		JBSS	0.96	0.43	0.51	1.76	1.23
	Considering γ_e and Ω_e (LX_5)	JPSS, OPSW	0.98	-0.25	0.98	0.40	0.28
		SPS	0.91	0.09	1.19	1.32	0.84
		JBSS	0.97	0.22	0.62	1.45	1.02

Table A1. Cont.

Inversion Models	PAI Estimation	Sub-Series Scenes	R ²	Intercept	Slope	RMSE	MAE
Considering γ_e and Ω_e (LX_15)		JPSS, OPSW	0.98	-0.29	0.86	0.73	0.62
		SPS	0.91	-0.62	1.25	1.10	0.82
		JBSS	0.96	0.11	0.57	1.77	1.34
Considering γ_e and Ω_e (LX_30)		JPSS, OPSW	0.98	-0.31	0.80	0.92	0.82
		SPS	0.92	-0.93	1.25	0.99	0.87
		JBSS	0.95	0.08	0.53	1.96	1.51
Considering γ_e and Ω_e (PCS)		JPSS, OPSW	0.86	2.51	1.22	3.28	3.23
		SPS	0.55	6.70	0.27	3.75	3.50
		JBSS	0.84	2.90	0.53	1.58	1.27
Considering γ_e and Ω_e (CC)		JPSS, OPSW	0.98	-0.11	0.89	0.51	0.37
		SPS	0.93	-0.79	1.38	1.40	0.68
		JBSS	0.93	-0.02	0.69	1.46	1.24
Considering γ_e and Ω_e (CLX_15)		JPSS, OPSW	0.98	-0.02	1.14	0.53	0.42
		SPS	0.91	0.65	1.33	2.40	1.85
		JBSS	0.95	0.34	0.75	0.93	0.61
Considering γ_e and Ω_e (CLX_30)		JPSS, OPSW	0.98	0.03	1.07	0.41	0.31
		SPS	0.91	0.31	1.37	2.25	1.62
		JBSS	0.95	0.32	0.72	1.04	0.74
Considering γ_e and Ω_e (CLX_45)		JPSS, OPSW	0.98	0.07	1.03	0.35	0.30
		SPS	0.92	0.04	1.40	2.14	1.30
		JBSS	0.94	0.31	0.70	1.11	0.81
Considering γ_e and Ω_e (LX_5)		JPSS, OPSW	0.98	-0.33	1.22	0.53	0.37
		SPS	0.91	0.58	1.36	2.49	1.93
		JBSS	0.96	0.11	0.82	0.83	0.54
Considering γ_e and Ω_e (LX_15)		JPSS, OPSW	0.98	-0.39	1.11	0.34	0.28
		SPS	0.92	-0.29	1.46	2.18	1.29
		JBSS	0.95	-0.0	0.76	1.13	0.92
Considering γ_e and Ω_e (LX_30)		JPSS, OPSW	0.98	-0.41	1.04	0.41	0.26
		SPS	0.92	-0.82	1.52	2.0	0.94
		JBSS	0.94	-0.04	0.73	1.31	1.12
Considering γ_e and Ω_e (PCS)		JPSS, OPSW	0.86	2.86	1.33	3.94	3.89
		SPS	0.77	7.10	0.43	4.72	4.64
		JBSS	0.88	2.85	0.71	1.96	1.79
Considering γ_e and Ω_e (CC)		JPSS, OPSW	0.98	0.02	0.76	0.77	0.63
		SPS	0.93	-1.12	1.30	1.01	0.91
		JBSS	0.95	0.26	0.54	1.79	1.33
Considering γ_e and Ω_e (CLX_15)		JPSS, OPSW	0.98	0.07	1.07	0.43	0.34
		SPS	0.92	-0.10	1.43	2.19	1.54
		JBSS	0.97	0.59	0.67	1.01	0.53
Considering γ_e and Ω_e (CLX_30)		JPSS, OPSW	0.98	0.16	0.98	0.32	0.27
		SPS	0.92	-0.37	1.44	1.97	1.28
		JBSS	0.96	0.57	0.63	1.17	0.68
Considering γ_e and Ω_e (CLX_45)		JPSS, OPSW	0.98	0.21	0.93	0.31	0.21
		SPS	0.92	-0.56	1.43	1.80	0.94
		JBSS	0.96	0.56	0.61	1.26	0.75
Considering γ_e and Ω_e (LX_5)		JPSS, OPSW	0.98	-0.30	1.16	0.40	0.31
		SPS	0.92	-0.18	1.47	2.26	1.54
		JBSS	0.98	0.29	0.75	0.89	0.57
Considering γ_e and Ω_e (LX_15)		JPSS, OPSW	0.98	-0.34	1.01	0.39	0.28
		SPS	0.92	-1.04	1.53	1.90	0.93
		JBSS	0.97	0.16	0.68	1.28	0.96
Considering γ_e and Ω_e (LX_30)		JPSS, OPSW	0.98	-0.34	0.93	0.58	0.51
		SPS	0.92	-1.38	1.52	1.60	0.87
		JBSS	0.96	0.13	0.63	1.52	1.19
Considering γ_e and Ω_e (PCS)		JPSS, OPSW	0.86	3.01	1.54	4.72	4.73
		SPS	0.54	8.21	0.31	5.35	5.27
		JBSS	0.83	3.75	0.64	2.60	2.50
Considering γ_e and Ω_e (CC)		JPSS, OPSW	0.98	-0.06	0.80	0.72	0.62
		SPS	0.91	-1.04	1.35	1.27	1.03
		JBSS	0.94	0.24	0.52	1.87	1.36
Considering γ_e and Ω_e (CLX_15)		JPSS, OPSW	0.98	0.13	1.03	0.37	0.30
		SPS	0.89	0.21	1.39	2.32	1.78
		JBSS	0.96	0.56	0.61	1.24	0.71
Considering γ_e and Ω_e (CLX_30)		JPSS, OPSW	0.98	0.16	0.96	0.30	0.22
		SPS	0.90	-0.11	1.40	2.12	1.48
		JBSS	0.96	0.52	0.59	1.38	0.84
Considering γ_e and Ω_e (CLX_45)		JPSS, OPSW	0.98	0.19	0.92	0.30	0.16
		SPS	0.90	-0.34	1.41	1.96	1.12
		JBSS	0.95	0.51	0.57	1.46	0.90

Table A1. Cont.

Inversion Models	PAI Estimation	Sub-Series Scenes	R ²	Intercept	Slope	RMSE	MAE
DHP_0-90	Considering γ_e and Ω_e (LX_5)	JPSS, OPSW	0.98	-0.21	1.12	0.36	0.28
		SPS	0.89	0.24	1.40	2.39	1.82
		JBSS	0.97	0.31	0.69	1.13	0.70
Considering γ_e and Ω_e (LX_15)	JPSS, OPSW	0.98	-0.30	1.01	0.38	0.25	
	SPS	0.90	-0.61	1.48	2.06	1.18	
	JBSS	0.96	0.19	0.64	1.45	1.05	
Considering γ_e and Ω_e (LX_30)	JPSS, OPSW	0.98	-0.33	0.95	0.54	0.44	
	SPS	0.90	-1.01	1.49	1.81	1.04	
	JBSS	0.95	0.15	0.60	1.64	1.23	
Considering γ_e and Ω_e (PCS)	JPSS, OPSW	0.86	3.05	1.29	4.02	4.02	
	SPS	0.55	7.67	0.35	5.04	4.87	
	JBSS	0.86	3.09	0.57	1.81	1.55	
Considering γ_e and Ω_e (CC)	JPSS, OPSW	0.98	0.03	0.72	0.87	0.73	
	SPS	0.91	-1.06	1.31	1.17	1.22	
	JBSS	0.95	0.25	0.49	2.0	1.50	
Considering γ_e and Ω_e (CLX_15)	JPSS, OPSW	0.97	0.17	0.93	0.31	0.19	
	SPS	0.90	-0.09	1.38	2.04	1.47	
	JBSS	0.96	0.53	0.58	1.39	0.85	
Considering γ_e and Ω_e (CLX_30)	JPSS, OPSW	0.97	0.21	0.88	0.35	0.19	
	SPS	0.90	-0.33	1.39	1.87	1.24	
	JBSS	0.96	0.50	0.56	1.52	0.96	
Considering γ_e and Ω_e (CLX_45)	JPSS, OPSW	0.97	0.24	0.84	0.41	0.21	
	SPS	0.90	-0.51	1.39	1.74	0.93	
	JBSS	0.96	0.49	0.54	1.59	1.01	
Considering γ_e and Ω_e (LX_5)	JPSS, OPSW	0.98	-0.13	1.02	0.29	0.19	
	SPS	0.90	-0.10	1.40	2.10	1.50	
	JBSS	0.97	0.30	0.65	1.29	0.85	
Considering γ_e and Ω_e (LX_15)	JPSS, OPSW	0.98	-0.20	0.91	0.52	0.41	
	SPS	0.90	-0.81	1.46	1.83	1.01	
	JBSS	0.96	0.19	0.60	1.60	1.16	
Considering γ_e and Ω_e (LX_30)	JPSS, OPSW	0.98	-0.22	0.86	0.69	0.58	
	SPS	0.90	-1.12	1.46	1.62	0.96	
	JBSS	0.95	0.16	0.56	1.78	1.33	
Considering γ_e and Ω_e (PCS)	JPSS, OPSW	0.87	2.69	1.23	3.49	3.42	
	SPS	0.69	6.61	0.47	4.43	4.19	
	JBSS	0.86	2.92	0.55	1.64	1.31	
Considering γ_e and Ω_e (CC)	JPSS, OPSW	0.97	-0.15	0.84	0.70	0.47	
	SPS	0.93	-1.78	1.51	1.36	0.72	
	JBSS	0.95	0.11	0.60	1.67	1.34	
Considering γ_e and Ω_e (CLX_15)	JPSS, OPSW	0.97	0.22	1.09	0.64	0.47	
	SPS	0.89	0.16	1.43	2.49	1.96	
	JBSS	0.97	0.65	0.66	1.00	0.50	
Considering γ_e and Ω_e (CLX_30)	JPSS, OPSW	0.97	0.30	1.0	0.45	0.36	
	SPS	0.90	-0.29	1.47	2.27	1.67	
	JBSS	0.96	0.56	0.63	1.17	0.67	
Considering γ_e and Ω_e (CLX_45)	JPSS, OPSW	0.97	0.33	0.94	0.39	0.30	
	SPS	0.91	-0.59	1.51	2.15	1.32	
	JBSS	0.96	0.52	0.62	1.25	0.75	
Considering γ_e and Ω_e (LX_5)	JPSS, OPSW	0.98	-0.31	1.23	0.59	0.39	
	SPS	0.90	-0.04	1.48	2.53	1.85	
	JBSS	0.97	0.29	0.76	0.87	0.48	
Considering γ_e and Ω_e (LX_15)	JPSS, OPSW	0.98	-0.34	1.06	0.38	0.24	
	SPS	0.91	-1.14	1.60	2.18	1.18	
	JBSS	0.96	0.15	0.69	1.25	0.89	
Considering γ_e and Ω_e (LX_30)	JPSS, OPSW	0.97	-0.36	0.99	0.51	0.42	
	SPS	0.92	-1.72	1.66	1.97	1.11	
	JBSS	0.96	0.12	0.65	1.44	1.11	
Considering γ_e and Ω_e (PCS)	JPSS, OPSW	0.82	3.52	1.57	5.38	5.33	
	SPS	0.47	8.53	0.25	5.46	5.34	
	JBSS	0.83	3.53	0.55	2.14	1.96	

All correlations are significant ($p < 0.05$, two-tailed t -test) except the combinations of inversion model, γ_e , Ω_e estimation algorithm, and segment size with PCS at the sub-series coniferous scenes of SPS. For each inversion model, the best two combinations of inversion model, γ_e , Ω_e estimation algorithm, and segment size to estimate the PAI of three groups of sub-series scenes are indicated in boldface and red color in Table A1.

Appendix C.1.2. Leaf-off Forest Scenes

Large differences were observed between the WAI derived from the combinations of inversion model, Ω_w estimation algorithm, and segment size with different inversion models but with the same Ω_w estimation algorithm, and segment size, and from the combinations with the same inversion model but with different Ω_w estimation algorithms and segment sizes (Table A2 and Figure 11). For example, Figure 11d shows large differences between the WAI estimated from the three combinations of LAI-2200 and CC, LAI-2200 and LX_5, and LAI-2200 and PCS at the leaf-off deciduous scenes (Table A2). Another evidence of the large differences between the WAI estimates of the three combinations are the significant differences between the RMSE, MAE, and regression slope of the three combinations, which are 0.32, 0.20, 0.72; 0.15, 0.07, 0.90, and 0.68, 0.66, and 1.22, respectively (Table A2). Similarly, the RMSE, MAE, and regression slope of the three combinations of Miller_10-65 and CC, Miller_0-80 and CC and 57.3 and CC are 0.74, 0.59, 0.42; 0.49, 0.34, 0.60, and 0.30, 0.18, and 0.76, respectively (Table A2). The obvious differences between the RMSE, MAE, and regression slope of the two groups of the three combinations of inversion model, Ω_w estimation algorithm and segment size indicate that the performance of the combination of inversion model, Ω_w estimation algorithm and segment size to estimate the WAI of leaf-off deciduous scenes strongly rely on the inversion model and Ω_w estimation algorithm used. No significant differences were observed between the WAI estimated from the combinations of inversion model, Ω_w estimation algorithm and segment size with the same inversion model and Ω_w estimation algorithm (LX and CLX) but with different segment sizes (Figure 11 and Table A2). For example, the mean variations in proportion between the WAI estimated from 57.3 and CLX_15 and those derived from 57.3 and CLX_30, and 57.3 and CLX_45 are 8% and 12%, respectively. Similarly, the mean variations in proportion between the WAI estimated from 57.3 and LX_5 and those derived from the two combinations of 57.3 and LX_15 and 57.3 and LX_30 are 9% and 12%, respectively. These results illustrate that the option of segment size is not the key factor that affects the performance of the combination of inversion model, Ω_w estimation algorithm, and segment size to estimate the WAI of leaf-off deciduous scenes.

The combinations of inversion model, Ω_w estimation algorithm, and segment size with LX and CLX performed better than the combinations with the same inversion model but with two other Ω_w estimation algorithms to estimate the WAI of leaf-off deciduous scenes, except the combinations with Miller_10-65, Miller_0-80, and DHP_0-90 (Table A2). The combination of inversion model, Ω_w estimation algorithm, and segment size with PCS tended to systematically overestimate the WAI at the leaf-off deciduous scenes except the combinations with Miller_10-65 (Figure 11).

Table A2. Correlation statistics between true and estimated WAI of leaf-off deciduous forest scenes estimated from seven inversion models considering G_w and Ω_w . The RMSE and MAE are expressed in WAI units (m^2/m^2).

Inversion Models	PAI Estimation	R^2	Intercept	Slope	RMSE	MAE
Miller_10-65	Considering Ω_w (CC)	0.99	0.05	0.42	0.74	0.59
	Considering Ω_w (CLX_15)	0.96	0.21	0.51	0.50	0.30
	Considering Ω_w (CLX_30)	0.96	0.25	0.45	0.55	0.35
	Considering Ω_w (CLX_45)	0.96	0.27	0.42	0.57	0.38
	Considering Ω_w (LX_5)	0.98	0.03	0.53	0.60	0.47
	Considering Ω_w (LX_15)	0.98	0.03	0.48	0.68	0.54
	Considering Ω_w (LX_30)	0.98	0.03	0.45	0.71	0.56
	Considering Ω_w (PCS)	0.98	0.21	0.76	0.23	0.10
Miller_0-80	Considering Ω_w (CC)	0.98	0.07	0.60	0.49	0.34
	Considering Ω_w (CLX_15)	0.97	0.25	0.69	0.27	0.17
	Considering Ω_w (CLX_30)	0.97	0.30	0.63	0.31	0.21
	Considering Ω_w (CLX_45)	0.97	0.31	0.60	0.34	0.21
	Considering Ω_w (LX_5)	0.98	0.05	0.74	0.32	0.22
	Considering Ω_w (LX_15)	0.98	0.04	0.67	0.41	0.29
	Considering Ω_w (LX_30)	0.98	0.04	0.64	0.45	0.32
	Considering Ω_w (PCS)	0.98	0.31	0.98	0.33	0.31

Table A2. Cont.

Inversion Models	PAI Estimation	R^2	Intercept	Slope	RMSE	MAE
Miller_0-90	Considering Ω_w (CC)	0.96	−0.03	0.82	0.32	0.21
	Considering Ω_w (CLX_15)	0.96	0.18	0.89	0.22	0.15
	Considering Ω_w (CLX_30)	0.95	0.21	0.83	0.23	0.17
	Considering Ω_w (CLX_45)	0.95	0.22	0.81	0.24	0.17
	Considering Ω_w (LX_5)	0.97	−0.06	0.95	0.21	0.12
	Considering Ω_w (LX_15)	0.96	−0.04	0.88	0.26	0.18
	Considering Ω_w (LX_30)	0.96	−0.05	0.86	0.29	0.18
	Considering Ω_w (PCS)	0.97	0.24	1.16	0.47	0.42
LAI-2200	Considering Ω_w (CC)	0.98	0.09	0.72	0.32	0.20
	Considering Ω_w (CLX_15)	0.97	0.33	0.84	0.24	0.18
	Considering Ω_w (CLX_30)	0.97	0.38	0.76	0.25	0.17
	Considering Ω_w (CLX_45)	0.97	0.40	0.73	0.26	0.16
	Considering Ω_w (LX_5)	0.98	0.07	0.90	0.15	0.07
	Considering Ω_w (LX_15)	0.98	0.06	0.81	0.23	0.14
	Considering Ω_w (LX_30)	0.98	0.05	0.77	0.28	0.19
	Considering Ω_w (PCS)	0.97	0.39	1.22	0.68	0.66
DHP_0-81	Considering Ω_w (CC)	0.98	0.08	0.69	0.36	0.22
	Considering Ω_w (CLX_15)	0.97	0.29	0.78	0.21	0.15
	Considering Ω_w (CLX_30)	0.97	0.32	0.72	0.24	0.16
	Considering Ω_w (CLX_45)	0.97	0.34	0.69	0.25	0.18
	Considering Ω_w (LX_5)	0.98	0.07	0.84	0.20	0.11
	Considering Ω_w (LX_15)	0.98	0.06	0.76	0.28	0.19
	Considering Ω_w (LX_30)	0.98	0.06	0.73	0.32	0.21
	Considering Ω_w (PCS)	0.98	0.37	1.07	0.48	0.47
DHP_0-90	Considering Ω_w (CC)	0.98	0.09	0.65	0.40	0.25
	Considering Ω_w (CLX_15)	0.97	0.28	0.74	0.23	0.15
	Considering Ω_w (CLX_30)	0.97	0.32	0.68	0.26	0.17
	Considering Ω_w (CLX_45)	0.97	0.33	0.65	0.28	0.18
	Considering Ω_w (LX_5)	0.98	0.08	0.79	0.24	0.14
	Considering Ω_w (LX_15)	0.98	0.07	0.72	0.33	0.21
	Considering Ω_w (LX_30)	0.98	0.07	0.69	0.37	0.24
	Considering Ω_w (PCS)	0.98	0.35	1.02	0.40	0.40
57.3	Considering Ω_w (CC)	0.98	0.05	0.76	0.30	0.18
	Considering Ω_w (CLX_15)	0.97	0.46	0.73	0.28	0.22
	Considering Ω_w (CLX_30)	0.97	0.46	0.66	0.29	0.16
	Considering Ω_w (CLX_45)	0.96	0.45	0.65	0.29	0.16
	Considering Ω_w (LX_5)	0.98	0.08	0.89	0.16	0.06
	Considering Ω_w (LX_15)	0.98	0.06	0.81	0.23	0.12
	Considering Ω_w (LX_30)	0.98	0.06	0.78	0.27	0.14
	Considering Ω_w (PCS)	0.97	0.44	1.16	0.67	0.65

All correlations are significant ($p < 0.05$, two-tailed t -test). For each inversion model, the best performance of the two combinations of inversion model, Ω_w estimation algorithm and segment size to estimate the WAI of leaf-off deciduous scenes are indicated in boldface and red color in Table A2.

Appendix C.2. The True PAI and WAI of Leaf-on and Leaf-off Forest Scenes

Scene PAI and WAI also affect the performance of the seven inversion models to estimate the PAI and WAI of leaf-on and leaf-off scenes. For leaf-on deciduous scenes, the PAI underestimation increased with the scene PAI obviously at the leaf-on deciduous forest scenes with PAI > 3.5 (Figure 9). A sign of this trend is that the regression slope of the PAI estimated from all the combinations of inversion model, γ_e , Ω_e estimation algorithm, and segment size at the leaf-on deciduous scenes are below one (Table A1). For leaf-on coniferous scenes, the seven inversion models, except Miller_10-65, overestimated PAI at the SPS coniferous scenes with PAI > 6.0 if γ_e and Ω_e were considered in the PAI estimation (Figure 8). All the seven inversion models except Miller_10-65 and Miller_0-90 tended to underestimate the WAI at the leaf-off deciduous scenes with WAI > 2.5, even though the Ω_w was considered in the WAI estimation (Figure 11).

Appendix C.3. The Reference Ω_e and Ω_w of Leaf-on and Leaf-off Scenes

Figure A1 show the mean $\Omega_e(\theta)$ of the six leaf-on coniferous scenes with reference $\Omega_e > 1$ and the mean $\Omega_w(\theta)$ of the five leaf-off deciduous scenes with reference $\Omega_w > 1$. The Ω_e and Ω_w estimates were derived using CC, CLX, LX, and PCS. All Ω_e estimation algorithms seem to overestimate the $\Omega_e(\theta)$ at zenith angles near 57.3° , especially for LX, CLX, and PCS (Figure A1a). Similarly, all Ω_w estimation algorithms overestimated the $\Omega_w(\theta)$ at zenith angles near 57.3° except CC (Figure A1b).

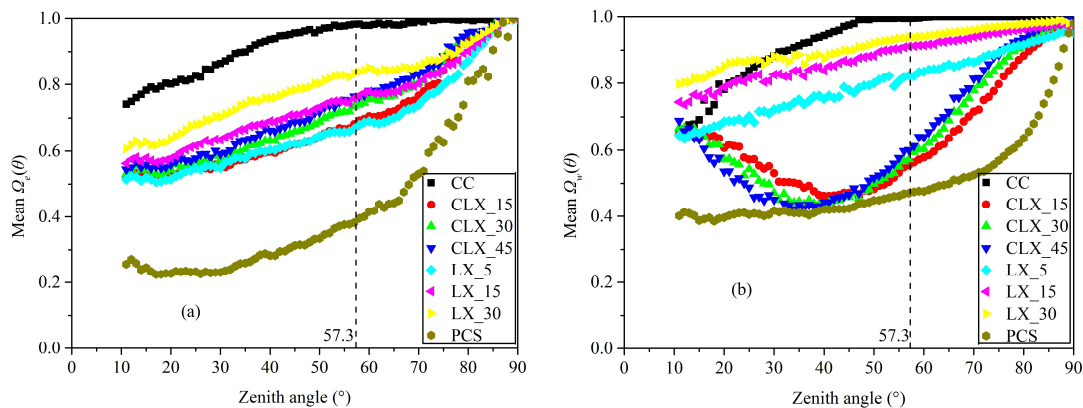


Figure A1. Mean $\Omega_e(\theta)$ and $\Omega_w(\theta)$ derived from CC, CLX, LX, and PCS at the six leaf-on coniferous scenes with reference $\Omega_e > 1$ (a) and five leaf-off deciduous scenes with reference $\Omega_w > 1$ (b), respectively.

References

1. Aber, J.; Neilson, R.P.; McNulty, S.; Lenihan, J.M.; Bachelet, D.; Drapek, R.J. Forest processes and global environmental change: Predicting the effects of individual and multiple stressors: We review the effects of several rapidly changing environmental drivers on ecosystem function, discuss interactions among them, and summarize predicted changes in productivity, carbon storage, and water balance. *BioScience* **2001**, *51*, 735–751.
2. Jonckheere, I.; Fleck, S.; Nackaerts, K.; Muys, B.; Coppin, P.; Weiss, M.; Baret, F. Review of methods for in situ leaf area index determination: Part I. Theories, sensors and hemispherical photography. *Agric. For. Meteorol.* **2004**, *121*, 19–35. [[CrossRef](#)]
3. Running, S.W.; Coughlan, J.C. A general model of forest ecosystem processes for regional applications I. Hydrologic balance, canopy gas exchange and primary production processes. *Ecol. Model.* **1988**, *42*, 125–154. [[CrossRef](#)]
4. Sellers, P.J.; Dickinson, R.E.; Randall, D.A.; Betts, A.K.; Hall, F.G.; Berry, J.A.; Collatz, G.J.; Denning, A.S.; Mooney, H.A.; Nobre, C.A.; et al. Modeling the exchanges of energy, water, and carbon between continents and the atmosphere. *Science* **1997**, *275*, 502–509. [[CrossRef](#)] [[PubMed](#)]
5. Watson, D.J. Comparative physiological studies in the growth of field crops: I. Variation in net assimilation rate and leaf area between species and varieties, and within and between years. *Ann. Bot.* **1947**, *11*, 41–76. [[CrossRef](#)]
6. Chen, J.M.; Black, T.A. Defining leaf area index for non-flat leaves. *Plant Cell Environ.* **1992**, *15*, 421–429. [[CrossRef](#)]
7. Ross, J. *The Radiation Regime and Architecture of Plant Stands*; Dr. W. Junk Publishers: The Hague, The Netherlands, 1981.
8. Zou, J.; Yan, G.; Zhu, L.; Zhang, W. Woody-to-total area ratio determination with a multispectral canopy imager. *Tree Physiol.* **2009**, *29*, 1069–1080. [[CrossRef](#)] [[PubMed](#)]
9. Bréda, N.J.J. Ground-based measurements of leaf area index: A review of methods, instruments and current controversies. *J. Exp. Bot.* **2003**, *54*, 2403–2417. [[CrossRef](#)] [[PubMed](#)]
10. Chen, J.M.; Rich, P.M.; Gower, S.T.; Norman, J.M.; Plummer, S. Leaf area index of boreal forests: Theory, techniques, and measurements. *J. Geophys. Res. Atmos.* **1997**, *102*, 29429–29443. [[CrossRef](#)]
11. Duursma, R.A.; Marshall, J.D.; Robinson, A.P. Leaf area index inferred from solar beam transmission in mixed conifer forests on complex terrain. *Agric. For. Meteorol.* **2003**, *118*, 221–236. [[CrossRef](#)]

12. Levy, P.E.; Jarvis, P.G. Direct and indirect measurements of lai in millet and fallow vegetation in hapex-sahel. *Agric. For. Meteorol.* **1999**, *97*, 199–212. [[CrossRef](#)]
13. Monsi, M.; Saeki, T. Über den lichtfaktor in den pflanzengesellschaften und seine bedeutung für die stoffproduktion. *Jpn. J. Bot.* **1953**, *14*, 22–52.
14. Nilson, T. A theoretical analysis of the frequency of gaps in plant stands. *Agric. Meteorol.* **1971**, *8*, 25–38. [[CrossRef](#)]
15. Weiss, M.; Baret, F.; Smith, G.J.; Jonckheere, I.; Coppin, P. Review of methods for in situ leaf area index (LAI) determination: Part II. Estimation of lai, errors and sampling. *Agric. For. Meteorol.* **2004**, *121*, 37–53. [[CrossRef](#)]
16. Chianucci, F.; Cutini, A. Estimation of canopy properties in deciduous forests with digital hemispherical and cover photography. *Agric. For. Meteorol.* **2013**, *168*, 130–139. [[CrossRef](#)]
17. Leblanc, S.G.; Chen, J.M.; Fernandes, R.; Deering, D.W.; Conley, A. Methodology comparison for canopy structure parameters extraction from digital hemispherical photography in boreal forests. *Agric. For. Meteorol.* **2005**, *129*, 187–207. [[CrossRef](#)]
18. Leblanc, S.G.; Fournier, R.A. Hemispherical photography simulations with an architectural model to assess retrieval of leaf area index. *Agric. For. Meteorol.* **2014**, *194*, 64–76. [[CrossRef](#)]
19. Miller, J. A formula for average foliage density. *Aust. J. Bot.* **1967**, *15*, 141–144. [[CrossRef](#)]
20. Cao, B.; Du, Y.; Li, J.; Li, H.; Li, L.; Zhang, Y.; Zou, J.; Liu, Q. Comparison of five slope correction methods for leaf area index estimation from hemispherical photography. *IEEE Geosci. Remote Sens. Lett.* **2015**, *12*, 1958–1962. [[CrossRef](#)]
21. Perry, S.G.; Fraser, A.B.; Thomson, D.W.; Norman, J.M. Indirect sensing of plant canopy structure with simple radiation measurements. *Agric. For. Meteorol.* **1988**, *42*, 255–278. [[CrossRef](#)]
22. Liu, Z.; Jin, G.; Chen, J.; Qi, Y. Evaluating optical measurements of leaf area index against litter collection in a mixed broadleaved-Korean pine forest in China. *Trees* **2015**, *29*, 59–73. [[CrossRef](#)]
23. Thimonier, A.; Sedivy, I.; Schleppei, P. Estimating leaf area index in different types of mature forest stands in Switzerland: A comparison of methods. *Eur. J. For. Res.* **2010**, *129*, 543–562. [[CrossRef](#)]
24. Macfarlane, C.; Grigg, A.; Evangelista, C. Estimating forest leaf area using cover and fullframe fisheye photography: Thinking inside the circle. *Agric. For. Meteorol.* **2007**, *146*, 1–12. [[CrossRef](#)]
25. Van Gardingen, P.R.; Jackson, G.E.; Hernandez-Daumas, S.; Russell, G.; Sharp, L. Leaf area index estimates obtained for clumped canopies using hemispherical photography. *Agric. For. Meteorol.* **1999**, *94*, 243–257. [[CrossRef](#)]
26. Gonsamo, A.; Walter, J.-M.N.; Pellikka, P. Sampling gap fraction and size for estimating leaf area and clumping indices from hemispherical photographs. *Can. J. For. Res.* **2010**, *40*, 1588–1603. [[CrossRef](#)]
27. Chianucci, F. Canopy Properties Estimation in Deciduous Forests with Digital Photography. Ph.D. Thesis, Università degli studi della Tuscia-Viterbo, Viterbo, Italy, 2013.
28. Neumann, H.H.; Den Hartog, G.; Shaw, R.H. Leaf area measurements based on hemispheric photographs and leaf-litter collection in a deciduous forest during autumn leaf-fall. *Agric. For. Meteorol.* **1989**, *45*, 325–345. [[CrossRef](#)]
29. LI-COR. *Lai-2000 Plant Canopy Analyzer Instruction Manual*; Li-cor Cor.: Lincoln, NE, USA, 1992.
30. LI-COR. *Lai-2200 Plant Canopy Analyzer Instruction Manual*; Li-cor Cor.: Lincoln, NE, USA, 2009.
31. Barclay, H.J.; Trofymow, J.A.; Leach, R.I. Assessing bias from boles in calculating leaf area index in immature douglas-fir with the LI-COR canopy analyzer. *Agric. For. Meteorol.* **2000**, *100*, 255–260. [[CrossRef](#)]
32. Cutini, A.; Matteucci, G.; Mugnozsa, G.S. Estimation of leaf area index with the LI-COR LAI 2000 in deciduous forests. *For. Ecol. Manag.* **1998**, *105*, 55–65. [[CrossRef](#)]
33. Ryu, Y.; Nilson, T.; Kobayashi, H.; Sonnentag, O.; Law, B.E.; Baldocchi, D.D. On the correct estimation of effective leaf area index: Does it reveal information on clumping effects? *Agric. For. Meteorol.* **2010**, *150*, 463–472. [[CrossRef](#)]
34. Leblanc, S.G.; Chen, J.M. *Tracing Radiation and Architecture of Canopies Trac Manual Version 2.1.3*; Natural Resources Canada: Ottawa, ON, Canada, 2002; p. 25.
35. Chen, J.M. Optically-based methods for measuring seasonal variation of leaf area index in boreal conifer stands. *Agric. For. Meteorol.* **1996**, *80*, 135–163. [[CrossRef](#)]
36. Pisek, J.; Sonnentag, O.; Richardson, A.D.; Möttus, M. Is the spherical leaf inclination angle distribution a valid assumption for temperate and boreal broadleaf tree species? *Agric. For. Meteorol.* **2013**, *169*, 186–194. [[CrossRef](#)]

37. Woodgate, W.; Disney, M.; Armston, J.D.; Jones, S.D.; Suarez, L.; Hill, M.J.; Wilkes, P.; Soto-Berelov, M.; Haywood, A.; Mellor, A. An improved theoretical model of canopy gap probability for leaf area index estimation in woody ecosystems. *For. Ecol. Manag.* **2015**, *358*, 303–320. [[CrossRef](#)]
38. Raabe, K.; Pisek, J.; Sonnentag, O.; Annuk, K. Variations of leaf inclination angle distribution with height over the growing season and light exposure for eight broadleaf tree species. *Agric. For. Meteorol.* **2015**, *214–215*, 2–11. [[CrossRef](#)]
39. Ryu, Y.; Sonnentag, O.; Nilson, T.; Vargas, R.; Kobayashi, H.; Wenk, R.; Baldocchi, D.D. How to quantify tree leaf area index in an open savanna ecosystem: A multi-instrument and multi-model approach. *Agric. For. Meteorol.* **2010**, *150*, 63–76. [[CrossRef](#)]
40. Macfarlane, C.; Arndt, S.K.; Livesley, S.J.; Edgar, A.C.; White, D.A.; Adams, M.A.; Eamus, D. Estimation of leaf area index in eucalypt forest with vertical foliage, using cover and fullframe fisheye photography. *For. Ecol. Manag.* **2007**, *242*, 756–763. [[CrossRef](#)]
41. Gonsamo, A.; Pellikka, P. The computation of foliage clumping index using hemispherical photography. *Agric. For. Meteorol.* **2009**, *149*, 1781–1787. [[CrossRef](#)]
42. Jonckheere, I.; Nackaerts, K.; Muys, B.; van Aardt, J.; Coppin, P. A fractal dimension-based modelling approach for studying the effect of leaf distribution on LAI retrieval in forest canopies. *Ecol. Model.* **2006**, *197*, 179–195. [[CrossRef](#)]
43. Walter, J.-M.N.; Fournier, R.A.; Soudani, K.; Meyer, E. Integrating clumping effects in forest canopy structure: An assessment through hemispherical photographs. *Can. J. Remote Sens.* **2003**, *29*, 388–410. [[CrossRef](#)]
44. Woodgate, W.; Armston, J.D.; Disney, M.; Jones, S.D.; Suarez, L.; Hill, M.J.; Wilkes, P.; Soto-Berelov, M. Quantifying the impact of woody material on leaf area index estimation from hemispherical photography using 3D canopy simulations. *Agric. For. Meteorol.* **2016**, *226–227*, 1–12. [[CrossRef](#)]
45. Woodgate, W. In-Situ Leaf Area Index Estimate Uncertainty in Forests: Supporting Earth Observation Product Calibration and Validation. Ph.D. Thesis, RMIT University, Melbourne, Australia, 2015.
46. Schleppi, P.; Conedera, M.; Sedivy, I.; Thimonier, A. Correcting non-linearity and slope effects in the estimation of the leaf area index of forests from hemispherical photographs. *Agric. For. Meteorol.* **2007**, *144*, 236–242. [[CrossRef](#)]
47. Gower, S.T.; Kucharik, C.J.; Norman, J.M. Direct and indirect estimation of leaf area index, fapar, and net primary production of terrestrial ecosystems. *Remote Sens. Environ.* **1999**, *70*, 29–51. [[CrossRef](#)]
48. Andreas, D.; Carsten, C.; Oliver, D.; Philipp, S. In realistic and interactive visualization of high-density plant ecosystems. In Proceedings of the First Eurographics Conference on Natural Phenomena, Dublin, Ireland, 30 August 2005; Galin, E., Poulin, P., Eds.; Eurographics Association: Dublin, Ireland, 2005; pp. 73–81.
49. Widlowski, J.-L.; Mio, C.; Disney, M.; Adams, J.; Andredakis, I.; Atzberger, C.; Brennan, J.; Busetto, L.; Chelle, M.; Ceccherini, G.; et al. The fourth phase of the radiative transfer model intercomparison (RAMI) exercise: Actual canopy scenarios and conformity testing. *Remote Sens. Environ.* **2015**, *169*, 418–437. [[CrossRef](#)]
50. Lintermann, B.; Deussen, O. Interactive modeling of plants. *IEEE Comput. Graph. Appl.* **1999**, *19*, 56–65. [[CrossRef](#)]
51. Leblanc, S.G.; Fournier, R.A. Measurement of forest structure with hemispherical photography. In *Hemispherical Photography in Forest Science: Theory, Methods, Applications*; Fournier, R.A., Hall, R.J., Eds.; Springer: Dordrecht, The Netherlands, 2017; pp. 53–83.
52. Gonsamo, A.; Pellikka, P. Methodology comparison for slope correction in canopy leaf area index estimation using hemispherical photography. *For. Ecol. Manag.* **2008**, *256*, 749–759. [[CrossRef](#)]
53. Disney, M.; Lewis, P.; Saich, P. 3D modelling of forest canopy structure for remote sensing simulations in the optical and microwave domains. *Remote Sens. Environ.* **2006**, *100*, 114–132. [[CrossRef](#)]
54. Sumida, A.; Nakai, T.; Yamada, M.; Ono, K.; Uemura, S.; Hara, T. Ground-Based Estimation of Leaf Area Index and Vertical Distribution of Leaf Area Density in a *Betula Ermanii* Forest. *SILVA FENN.* **2009**, *43*, 799–816.
55. Walter, J.M.N.; Himmler, C.G. Spatial heterogeneity of a scots pine canopy: An assessment by hemispherical photographs. *Can. J. For. Res.* **1996**, *26*, 1610–1619. [[CrossRef](#)]
56. Zou, J.; Yan, G.; Chen, L. Estimation of canopy and woody components clumping indices at three mature *Pinus crassifolia* forest stands. *IEEE J. Sel. Top. Appl. Earth Obs. Remote Sens.* **2015**, *8*, 1413–1422. [[CrossRef](#)]
57. Lang, A.R.G.; Yueqin, X. Estimation of leaf area index from transmission of direct sunlight in discontinuous canopies. *Agric. For. Meteorol.* **1986**, *37*, 229–243. [[CrossRef](#)]

58. Chen, J.M.; Cihlar, J. Plant canopy gap-size analysis theory for improving optical measurements of leaf-area index. *Appl. Opt.* **1995**, *34*, 6211–6222. [[CrossRef](#)] [[PubMed](#)]
59. Chen, J.M.; Cihlar, J. Quantifying the effect of canopy architecture on optical measurements of leaf area index using two gap size analysis methods. *IEEE Trans. Geosci. Remote Sens.* **1995**, *33*, 777–787. [[CrossRef](#)]
60. Pisek, J.; Lang, M.; Nilson, T.; Korhonen, L.; Karu, H. Comparison of methods for measuring gap size distribution and canopy nonrandomness at Järvelja RAMI (radiation transfer model intercomparison) test sites. *Agric. For. Meteorol.* **2011**, *151*, 365–377. [[CrossRef](#)]
61. Chen, J.M. Remote sensing of leaf area index of vegetation covers. In *Remote Sensing of Natural Resources*; CRC Press: Boca Raton, FL, USA, 2013; pp. 375–398.
62. Baret, F.; de Solan, B.; Lopez-Lozano, R.; Ma, K.; Weiss, M. Gai estimates of row crops from downward looking digital photos taken perpendicular to rows at 57.5° zenith angle: Theoretical considerations based on 3D architecture models and application to wheat crops. *Agric. For. Meteorol.* **2010**, *150*, 1393–1401. [[CrossRef](#)]
63. Pisek, J.; Ryu, Y.; Alikas, K. Estimating leaf inclination and g-function from leveled digital camera photography in broadleaf canopies. *Trees* **2011**, *25*, 919–924. [[CrossRef](#)]
64. Kucharik, C.J.; Norman, J.M.; Gower, S.T. Measurements of branch area and adjusting leaf area index indirect measurements. *Agric. For. Meteorol.* **1998**, *91*, 69–88. [[CrossRef](#)]
65. Brendan, L.; Przemyslaw, P. Generating spatial distributions for multilevel models of plant communities. In *Proceedings of the Graphics Interface 2002*, Calgary, AB, Canada, 27–29 May 2002; pp. 69–80.
66. Majasalmi, T.; Rautiainen, M.; Stenberg, P.; Rita, H. Optimizing the sampling scheme for LAI-2000 measurements in a boreal forest. *Agric. For. Meteorol.* **2012**, *154–155*, 38–43. [[CrossRef](#)]
67. Nackaerts, K.; Coppin, P.; Muys, B.; Hermy, M. Sampling methodology for lai measurements with LAI-2000 in small forest stands. *Agric. For. Meteorol.* **2000**, *101*, 247–250. [[CrossRef](#)]



© 2018 by the authors. Licensee MDPI, Basel, Switzerland. This article is an open access article distributed under the terms and conditions of the Creative Commons Attribution (CC BY) license (<http://creativecommons.org/licenses/by/4.0/>).